Geol Rundsch (1998) 87: 2–20

ORIGINAL PAPER

M. Frechen · A. E. Dodonov

Loess chronology of the Middle and Upper Pleistocene in Tadjikistan

Received: 18 August 1997 / Accepted 23 December 1997

Abstract The loess/paleosol sequences of Central Asia are continuous terrestrial records of the Quaternary period and enable detailed comparison with paleoclimatic archives such as marine and ice core records in order to reconstruct regional and global paleoclimatic and paleoecological development during the past 130 000 years. Thermoluminescence (TL) and infrared stimulated luminescence (IRSL) dating methods are applied to the extensively studied loess/paleosol sequence of the section at Darai Kalon/Chashmanigar, Tadjikistan, in order to determine a more accurate chronological framework and climatostratigraphic reconstruction for the last interglacial/glacial cycle. Luminescence dating suggests that the loess above the first pedocomplex from the top, PC1, accumulated during the last glacial period. A high accumulation rate of up to 1.20 m per 1000 years was determined for the last glacial loess, especially for the uppermost 5–8 m. PC1 formed during the last interglacial period (oxygen-isotope stage 5). The loess between PC1 and PC2 is designated to be of penultimate glacial deposition age. Infrared stimulated luminescence and TL age estimates are in agreement to 80 000 years before present (BP), indicating a long-distance transport of the aeolian dust prior to deposition. The upper numerical age-limit range is between 300 000 and 450 000 years. However, reliable dating of the loess older than 130 000 years is not possible due to age scatter between samples and an inadequate increase of paleodose with depth. This high-resolution dating study underlines the importance of the section at Darai Kalon and indicates that it is one of the most continuous loess/paleosol records of the Northern Hemisphere. The chronological results are particularly important for the reconstruction of the human evolution in Central Asia, suggesting much older age estimates than previously obtained for most of the archeological key sites associated with PC5 and PC4 in Tadjikistan.

Key words Loess · Paleosols · Chronology · Central Asia · Tadjikistan · Luminescence dating · Pleistocene · Accumulation rates · Stratigraphy · Paleoclimate

M. Frechen (✉)
Center for Environmental Change and Quaternary Research, Cheltenham and Gloucester CHE, Francis Close Hall, Swindon Road, Cheltenham GL50 4AZ, UK
e-mail: mfrechen@chelt.ac.uk

A. E. Dodonov
Geological Institute, Russian Academy of Sciences, Pyzhevsky 7, 109017 Moscow, Russia

Introduction

During the Quaternary period continuous accumulation of dust formed widespread and thick loess deposits in periglacial areas of the northern and southern hemisphere. Loess/paleosol sequences indicate a high sensitivity in recording the regional paleoclimatic and paleoecological changes from land sites and show a close relationship with cooling and warming trends during the Quaternary. In general, loess is regarded to be representative of cold and dry periglacial climate and environment, whereas the intercalated paleosols are indicators of warmer and more humid climate, representing interstadial or interglacial periods. The loess/paleosol sequences of Central Asia and China are continuous terrestrial records of the Quaternary enabling a detailed comparison with paleoclimate proxy data from ocean sediments and ice cores. In Central Asia, South Tadjikistan is one of the key areas for loess investigations and is situated within the Afghan/Tadjic depression bordered by the Tien Shan Mountains to the north and northeast, by the western Pamir Mountains to the east and by the Hindukush Mountains to the south. The accumulation of dust occurs within the piedmont regions of the mountains. Thick loess deposits also exist around Samarkand and Tashkent in Usbekistan (Fig. 1).

In southern Tadjikistan loess is a widespread sediment on alluvial terraces in piedmont plains, covering slopes and interfluves to an elevation of 2500 m above sea level (a.s.l.). The loess attains here a thickness of up to 200 m.

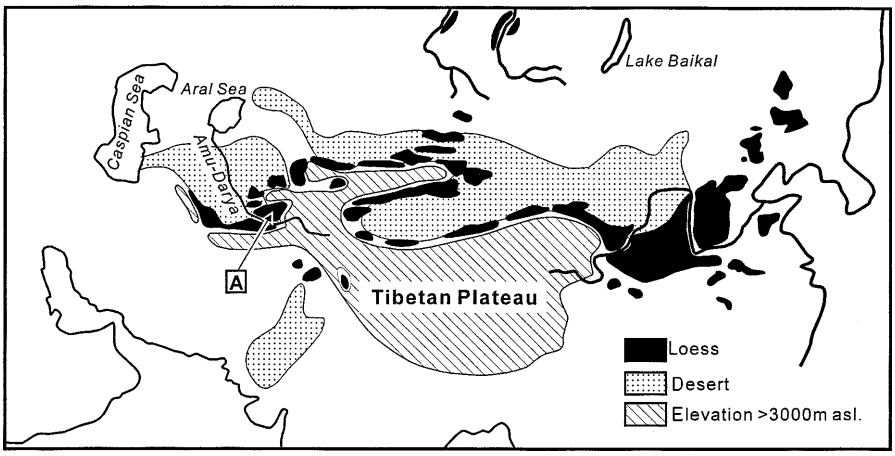

Fig. 1 Map showing the distribution of loess (*black*) and deserts (*dotted*) in Central Asia. The area of interest is marked with an *A*

The clayey, silty and fine sandy material derives from weathered rock surfaces from the deserts to the west, from frost shattering in high mountains or from glaciofluvial/fluvial deposits of the river floodplains. During modern dust storms there is dust convection up to altitudes of 2000 m a.s.l. It is suggested that during glacial conditions wind intensities were much stronger. Additionally, precipitation was reduced resulting in a large amount of dust accumulation. The deflation areas of the fine silty sediments are to the southwest and west of the Afghan/Tadjic depression where extended deserts, such as the Kyzyl Kum, and floodplains of big rivers, such as the Amu Darya, exist.

The loess/paleosol sequences of South Tadjikistan are similar to those of the well-studied central Loess Plateau in China (Dodonov 1991; Kukla and An 1989; Liu 1988, 1991). However, if the records are compared in detail, the chronological interpretation of loess stratigraphy in Central Asia and China has been different. Shackleton et al. (1995) pointed out that for the section at Karamaydan, South Tadjikistan, the patterns of magnetic susceptibility are similar to those from China and to the marine oxygen-isotope record for the Brunhes magnetochron. This is in contrast to the chronostratigraphic interpretation suggesting that in Central Asia most of the Aeolian deposits accumulated within the past 300 000 years and indicating a much lower accumulation rate before that time (Dodonov 1991; Lazarenko 1984). The loess/paleosol sequence either above PC3 or PC4 was considered to represent a detailed record of the past 130 000 years, recording climatic changes since the last interglacial optimum, correlated with oxygen-isotope substage 5e (Dodonov 1991; Lazarenko 1984). This stratigraphic interpretation results in chronostratigraphic and chronological problems for paleoclimatic reconstruction, for correlation with the Chinese loess/paleosol record and for archeological horizons of Early Paleolithic association (Dodonov et al. 1995; Schäfer et al. 1996). The interpretation was supported by earlier thermoluminescence dating that is no longer regarded as valid (Hütt and Smirnov 1984; Wintle and Huntley 1982; Zhou et al. 1995). Thus, an independent and reliable chronological framework for the last interglacial/glacial cycle is needed for the loess record in Tadjikistan.

As part of a transect between northwestern Europe and China, combined luminescence dating of European and Central Asian loess/paleosol sequences was carried out (Frechen, in press). The pedological and micromorphological investigations of sections Chashmanigar and Karamaydan were described by Bronger et al. (1995). Archeological investigations for the sections at Lakhuti and Khonako were provided by Schäfer et al. (1996). Seventy-four samples were collected from the type section at Darai Kalon near Chashmanigar in South Tadjikistan (Fig. 2) for a high-resolution study. The samples were systematically investigated by combined luminescence dating resulting in 296 infrared stimulated luminescence (IRSL) and thermoluminescence (TL) age determinations. Independent age

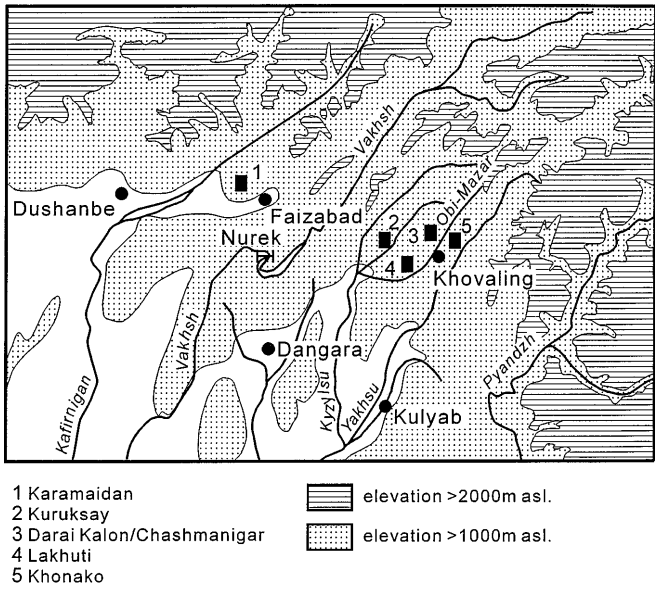

Fig. 2 Map showing the area of interest and the location of the section at Darai Kalon/Chashmanigar to the north of the settlement Khovaling

control is established by the position of the Brunhes/Matuyama (B/M) paleomagnetic boundary as described for the Karamaydan (Foerster and Heller 1994; Pen`kov and Gamov 1980) and Darai Kalon/Chashmanigar profiles (Pen`kov and Gamov 1980). According to paleomagnetic data the Brunhes/Matuyama polarity reversal is located in the loess between PC9 and PC10.

Central Asian loess stratigraphy

The Asian loess studies began last century (Richthofen 1878). Most of the earliest publications (in Russian) on loess were focused on the problems of loess genesis. Three main genetic approaches were initiated in order to explain loess features: aeolian, fluvial, and pedological. Following Richthofen, Obruchev (1885, 1900–1901, 1911, 1948) developed an aeolian theory. Pavlov (1903) compiled a fluvial hypothesis for loess-forming processes. Berg (1947) suggested pedological processes to describe loess strata. Being in competition, all of these theoretical principles were elaborated upon for many years, and numerous publications on Central Asian loess exist. More recently, the stratigraphy of the alternating Pleistocene loess/paleosol sequences was described (Dodonov 1979, 1991, 1995; Dodonov and Pen`kov 1977; Dodonov et al. 1977, 1995; Lazarenko 1984; Lazarenko et al. 1981; Pen`kov et al. 1976; Stepanov and Abdunazarov 1977). According to paleomagnetic data provided by Pen`kov, the Brunhes/Matuyama boundary was recognized in many loess/paleosol sequences between pedocomplexes (PC) 9 and 10, the Jaramillo subchron between PC15 and PC16, and the Olduvai subchron was found at the level of PC33 and PC34 (Dodonov and Pen`kov 1977; Pen`kov et al. 1976). The same stratigraphic position for the B/M boundary was confirmed in the Karamaydan section by Foerster and Heller (1994). Detailed descriptions of paleosols at the sections in Karamaydan and Chashmanigar demonstrate a nearly complete paleoclimatic record comparable with loess sections in China (Bronger et al. 1995). The stratigraphic subdivisions for loess/paleosol sequences in the Brunhes epoch were previously determined by counting paleosol horizons from the top and applying thermoluminescence dating measured in the TL laboratory of Kiev (Dodonov 1995; Lazarenko 1984). Previous investigations placed the stratigraphic position of the last interglacial paleosol at the level of the third pedocomplex (Lazarenko 1984) or at PC3 and PC4 (Dodonov 1991, 1995). In this study we used the same numbering scheme for pedocomplexes as Lazarenko (1984), Bronger et al. (1995) and Foerster and Heller (1994).

The stratigraphic correlation between loess/paleosol sequences from Tadjikistan and China, as well as with the marine oxygen-isotope record, revealed some contradiction and underestimation of TL dates for the upper five pedocomplexes in the Tadjikistan sections (Shackleton et al. 1995; Zhou et al. 1995a; Dodonov and Baiguzina 1995). Likewise, the problems with counting of loess and paleosols from the top, supported by invalid and underestimated TL dates, have been outlined for the Central European loess record (Frechen 1991, 1992; Frechen et al., in press).

A reliable chronology for the upper paleosols in Tadjikistan is desirable for reconstruction of early human evolution, considering the many Paleolithic sites discovered in pedocomplexes PC5, PC4, PC3, and PC2 (Ranov 1995). Owing to low field magnetic susceptibility variations at the section at Karamaydan, Foerster and Heller (1994) and Shackleton et al. (1995) correlated PC1 with paleosol S1 in China as well as with oxygen-isotope stage (OIS) 5. These results were confirmed by preliminary combined IRSL and TL dating (Frechen 1995) and TL measurements (Zhou et al. 1995b).

Luminescence dating methods

Comprehensive reviews of the "state-of-the-art" of luminescence principles, applications and limitations are provided by Aitken (1985), Wintle (1990, 1994), Frechen (1991, 1992) and Frechen et al. (1995, and in press). Aeolian sediments, such as loess and dune sands, are particularly suitable for the application of luminescence dating methods, enabling the determination of the last exposure to sunlight.

Thermoluminescence and IRSL is the light emitted from crystals such as quartz, feldspar, or zircon, when they are stimulated with heat or infrared light after receiving a natural or artificial dose of radiation. As a result of natural radiation in sediments, the number of electrons migrating to traps, connected to some type of impurities and crystal lattice defects, increases with time and radiation dose. The paleodose, accumulated or equivalent dose (ED), is a measure of the past radiation absorbed and, in combination with the dose rate, yields the time passed since the last exposure to sunlight. The equivalent dose is determined by measuring the fine-grained material using thermal and optical stimulations:

1. Thermal stimulation: luminescence using a continuous heating rate of 5 °C/s up to 450 °C
2. Optical stimulation: luminescence during exposure to radiation from infrared light diodes (880±80 nm wavelength)

Natural radiation results from the radioactive decay of isotopes in the decay chains of ^{235}U, ^{238}U, ^{232}Th, decay of ^{40}K, some minor isotopes including ^{87}Rb and cosmic rays. The luminescence age equals equivalent dose divided by dose rate.

An important assumption for IRSL and TL dating techniques is that the luminescence signal of the mineral grains was bleached and reset to near zero prior to sedimentation. From what is known about loess and aeolian dust (Pye 1987; Pécsi and Richter 1996) it might be assumed that the aeolian transport from the dust source to the area of deposition, e.g., Central Asia (Dodonov 1991), would guarantee a complete bleaching of the sediment to a negligible level for TL, and to zero for IRSL. However, in Central Europe significant differences in IRSL and TL paleodose determination have been described for loess and

loess derivatives (Frechen et al. 1995; Frechen and Preusser 1996). Significantly different transportation histories or sedimentary processes could be responsible for the diverse levels of depletion of the accumulated signal in minerals prior to sedimentation. Such transportation or deposition histories might result in incomplete bleaching; for example, transportation occurred in darkness or there was only a short distance of transport, which could result in depletion of the more sensitive IRSL signals, whereas the TL signal would be incompletely bleached. However, Frechen et al. (1995) and Musson and Wintle (1994) describe the considerable improvements for dating if both IRSL and TL are applied for paleodose determinations.

Experimental details

In the laboratory the following processes are simulated: Bleaching of the quartz and feldspar grains is done by artificial ultraviolet light or natural sunlight. Natural radioac-

Table 1 Dose rate data using gammaspectrometry in the laboratory

Sample	Uranium (ppm)	Thorium (ppm)	Potassium %	a efficiency IRSL	Dose rate IRSL (µGy/a)	a efficiency TL	Dose rate TL (µGy/a)
DRK201	2.42±0.17	9.05±0.63	1.31±0.07	0.068	2945±236	0.079	3055±248
DRK202	2.69±0.19	9.36±0.66	1.31±0.07	0.070		0.095	
DRK203	2.54±0.18	9.23±0.65	1.28±0.06	0.069	2990±240	0.091	3218±266
DRK204	2.79±0.20	9.68±0.68	1.36±0.07	0.070	3198±259	0.088	3398±281
DRK205	2.82±0.20	10.19±0.71	1.45±0.07	0.075	3390±275	0.085	3505±288
DRK206	2.78±0.19	10.60±0.74	1.49±0.07	0.065	3334±266	0.077	3474±282
DRK207	2.66±0.19	10.23±0.72	1.58±0.07	0.072	3409±273	0.087	3576±292
DRK208	2.49±0.17	9.32±0.65	1.45+0.07	0.085	3285±261	0.102	3460±281
DRK209	2.55±0.18	9.58±0.67	1.53±0.08	0.071	3252±261	0.093	3485±288
DRK210	2.73±0.19	9.54±0.67	1.49±0.07	0.075	3322±262	0.100	3596±294
DRK211	2.77±0.19	9.70±0.68	1.46±0.07	0.077	3351±271	0.100	3607±301
DRK212	2.81±0.20	9.48±0.66	1.49±0.07	0.060	3179±252	0.070	3290±264
DRK213	2.61±0.18	9.53±0.67	1.49±0.07	0.071	3236±259	0.104	3588±299
DRK214	2.50±0.18	9.64±0.68	1.49±0.07	0.071	3209±257	0.099	3503±290
DRK215	2.66±0.19	9.68±0.68	1.55±0.08	0.062	3219±256	0.088	3502±288
DRK216	2.70±0.19	9.09±0.64	1.48±0.07	0.052	3098±245	0.051	3098±245
DRK217	2.72±0.19	9.34±0.65	1.55±0.08	0.071	3303±265	0.099	3606±299
DRK218	2.58±0.18	8.93±0.62	1.47±0.07	0.073	3169±253	0.101	3457±286
DRK219	2.54±0.18	9.20±0.64	1.49±0.07	0.114	3623±305	0.094	3416±281
DRK220	2.70±0.19	9.18±0.64	1.48±0.07	0.063	3138±249	0.090	3426±281
DRK221	2.67±0.19	9.57±0.67	1.58±0.08	0.073	3355±270	0.090	3539±291
DRK222	2.84±0.20	9.50±0.67	1.62±0.08	0.061	3307±262	0.082	3541±288
DRK223	2.60±0.18	9.65±0.68	1.56±0.08	0.081	3408±277	0.105	3666±306
DRK224	2.60±0.18	9.69±0.68	1.57±0.07				
DRK225	2.77±0.19	9.45±0.66	1.57±0.08	0.066	3294±263	0.073	3370±271
DRK226	2.72±0.19	9.52±0.67	1.55±0.08	0.074	3354±271	0.098	3616±300
DRK227	2.71±0.19	9.31±0.65	1.50±0.08	0.069	3235±260	0.087	3429±282
DRK228	2.54±0.18	9.42±0.66	1.52±0.08	0.060	3109±247	0.076	3277±265
DRK229	2.48±0.17	8.55±0.60	1.40±0.07	0.076	3067±246	0.097	3274±270
DRK230	2.62±0.18	9.10±0.64	1.40±0.07	0.066	3071±245	0.079	3206±260
DRK231	2.64±0.18	10.08±0.71	1.53±0.08	0.071	3335±268	0.080	3434±280
DRK232	2.77±0.19	10.01±0.70	1.56±0.08	0.068	3363±270	0.093	3645±301
DRK233	2.80±0.20	10.34±0.72	1.62±0.08	0.076	3547±287	0.097	3789±315
DRK234	2.90±0.20	10.48±0.73	1.64±0.08		3661±298		3661±298
DRK235	3.13±0.22	11.49±0.80	1.76±0.09	0.066	3771±304	0.079	3938±322
DRK236	3.10±0.22	11.76±0.82	1.78±0.09	0.074		0.084	
DRK237	3.43±0.24	11.84±0.83	1.80±0.09	0.076	4076±333	0.087	4226±350
DRK238	3.45±0.24	12.18±0.85	1.89±0.09	0.075	4178±340	0.089	4372±362
DRK239	2.85±0.20	9.61±0.67	1.35±0.07	0.073	3237±263	0.090	3428±285
DRK240	3.05±0.21	11.18±0.78	1.51±0.08	0.061	3449±277	0.072	3586±292
DRK241	2.47±0.17	10.10±0.71	1.39±0.07	0.075	3197±259	0.091	3368±279
DRK242	2.43±0.17	9.79±0.69	1.52±0.08	0.069	3193±257	0.085	3360±275
DRK243	2.45±0.17	9.54±0.67	1.45±0.07	0.067	3097±247	0.088	3315±272
DRK244	2.46±0.17	10.66±0.75	1.63±0.08	0.076	3457±280	0.092	3632±299
DRK245	2.52±0.18	10.17±0.71	1.70±0.09	0.060	3310±264	0.070	3419±275
DRK246	2.72±0.19	11.51±0.81	1.73±0.09	0.073	3684±299	0.092	3912±325
DRK247	2.54±0.18	11.68±0.82	1.67±0.08	0.070	3544±286	0.083	3696±304
DRK248	2.23±0.16	9.97±0.70	1.62±0.08	0.072	3243±261	0.092	3446±283
DRK249	2.42±0.17	9.45±0.66	1.49±0.07	0.071	3141±252	0.097	3407±282
DRK250	2.57±0.18	10.39±0.73	1.63±0.08	0.059	3270±260	0.067	3358±270

For continuation of Table 1 please see the next page

Table 1 (Continued)

Sample	Uranium (ppm)	Thorium (ppm)	Potassium %	a efficiency IRSL	Dose rate IRSL (µGy/a)	a efficiency TL	Dose rate TL (µGy/a)
DRK251	2.33±0.16	9.05±0.16	1.31±0.07	0.067	2846±225	0.074	2973±239
DRK252	2.66±0.19	10.02±0.70	1.46±0.07	0.066	3204±258	0.071	3259±264
DRK253	2.86±0.20	9.32±0.65	1.45±0.07	0.067	3205±258	0.071	3249±263
DRK254	2.47±0.17	9.34±0.65	1.51±0.08	0.063	3072±246	0.077	3216±262
DRK255	3.03±0.21	11.23±0.79	1.76±0.09	0.070	3731±304	0.077	3819±313
DRK256	2.47±0.17	9.41±0.66	1.46±0.07	0.070	3110±250	0.080	3213±262
DRK257	2.42±0.17	9.66±0.68	1.55±0.08	0.070	3191±258	0.080	3294±269
DRK258	2.35±0.16	9.85±0.69	1.56±0.08	0.070	3194±258	0.082	3297±269
DRK259	2.41±0.17	9.64±0.67	1.51±0.08				
DRK260	2.42±0.17	9.64±0.67	1.59±0.08	0.063	3149±252	0.065	3170 ± 254
DRK261	2.22±0.16	8.99±0.63	1.52±0.08	0.072	3049±246	0.083	3154±258
DRK262	2.54±0.18	9.60±0.67	1.56±0.08	0.064		0.079	
DRK263	2.57±0.18	10.72±0.75	1.83±0.09	0.066	3532±275	0.079	3678±290
DRK264	2.48±0.17	0.38±0.66	1.55±0.08	0.070	3184±257	0.069	3173±256
DRK265	2.26±0.16	8.49±0.59	1.40±0.07	0.067	2868±230	0.058	2783±221
DRK266	2.26±0.16	8.76±0.61	1.44±0.07	0.059	2851±226	0.057	2832±224
DRK267	2.23±0.16	9.24±0.65	1.54±0.08				
DRK268	2.29±0.16	9.40±0.66	1.50±0.08	0.066	3039±245	0.080	3179±260
DRK269	2.30±0.16	9.30±0.67	1.52±0.08	0.070	3089±250	0.100	3386±283
DRK270	2.31±0.16	10.21±0.71	1.60±0.08	0.059	3134±249	0.057	3114±247
DRK271	2.19±0.15	10.17±0.71	1.54±0.08	0.071	3165±256	0.083	3287±269
DRK272	2.27±0.16	8.66±0.61	1.43±0.07	0.078	3017±245	0.098	3206±266
DRK273	2.43±0.17	10.28±0.72	1.68±0.08		3448±280		3630±300
DRK274	2.05±0.14	7.76±0.54	1.24±0.06	0.078	2688±217	0.095	2833±233

tivity is simulated by beta or gamma irradiation. As the ionization density of alpha irradiation is substantially less (Aitken 1985), the alpha effectiveness is estimated by comparing alpha with beta or gamma irradiation. The dose rate is subsequently determined assuming radioactive equilibrium for the sediments. All measurements were carried out on the 4 to 11 µm grain-size fraction using the preparation technique described by Frechen (1991) and Frechen et al. (1996). Bleaching was carried out for 16 h using an ultraviolet l amp (Osram Ultra-Vitalux 300 Watt). Samples were irradiated using a ^{60}Co source (dose rate between 8.5 and 9.5 Gy per minute) in eight different dose steps (five subsample discs per dose step) for all samples. Alpha irradiation was undertaken by a ^{241}Am source to determine the alpha effectiveness. After irradiation all aliquots were preheated at 150 °C for 16 h on a heating plate in order to eliminate the unstable part of the IRSL and TL signals (Aitken 1992; Frechen 1991). All discs were left at room temperature for at least 4 weeks after irradiation and at least 48 h between preheating and IRSL and TL measurements. Measurements were carried out using an automated Risø TL/OSL Reader (Bøtter-Jensen et al. 1991). A filter combination of Schott BG-39 and Chance Pilkington HA-3 was placed between the photomultiplier and aliquots for both IRSL and TL. After the 25 s of IR decay, the same discs were measured immediately by TL, using a heating rate of 5 °C/s up to 450 °C. Equivalent doses were obtained by regeneration and additive dose methods by integrating the 10 to 25 s range of the IR decay curve and the 300–400 °C range of the TL glow curve. An exponential growth curve was fitted for the different dose steps and compared with the natural luminescence signals to estimate the equivalent dose. Dose rates for all samples were obtained from potassium (potassium-40 at 1460.8 keV), uranium (lead-214 at 295.2 and 351.9 keV and bismuth-214 at 609.3 and 1120.3 keV) and thorium (actinium-228 at 338.3 and 911.1 keV, thallium-208 at 583.2 and 2614.5 keV, bismuth-212 at 727.3 keV) content, as measured by gamma spectrometry in the laboratory (Frechen 1991), assuming a water content of 15±5% (Table 1). The measured in situ water content for the upper part of the section at Darai Kalon was below 5% due to decades of exposure at the loess bluff and the past summer. The natural moisture was found to be between 15 and 20% at a depth of more than 20 m at Darai Kalon. Short-term fading tests were carried out by measuring and comparing the IR decay curves and glow curves at 4 weeks and more than 12 weeks after irradiation. A few samples were stored for more than 1 year after irradiation. The results indicate no detectable signal loss due to fading for both IRSL and TL. No change in signal intensity occurred above the average disc-to-disc scatter of ±10%.

Site geology

The section at Darai Kalon is located 15 km north of the settlement Khovaling at an altitude of approximately 2100 m a.s.l. (Fig. 2). The section at Chashmanigar is a few hundred meters away, but its lower part is buried by a

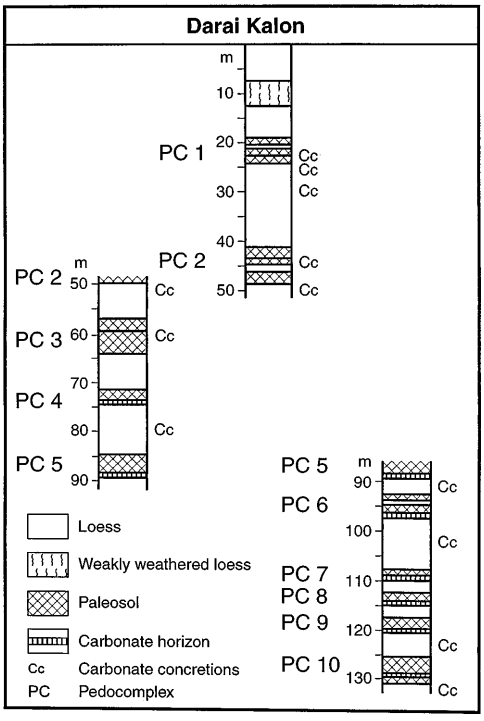

Fig. 3 The section at Darai Kalon consists of three individual profiles with a composite thickness of more than 130 m. The horizontal distance between each profile is less than 30 m. All three profiles can be correlated

huge landslide. At the section at Darai Kalon the cover sediments have a thickness of approximately 180 m. During the field work in autumn 1994 there were 138 m exposed in three profiles extending down to PC10 (Fig. 3). The loess/paleosol sequence above the B/M boundary has a thickness of 123 m including nine pedocomplexes, most of which consist of more than two paleosols. The loess has a pale yellowish color, a fine silty grain size and is rich in carbonates ranging from 13.58 to 27.51%. In the lower part the loess has little porosity.

The lowermost part of the section consists of fine silty, dense, pale yellowish loess rich in carbonate. Manganese and iron hydroxides are sometimes intermingled in the loess. Between 137.80 and 137.50 an enrichment of badly preserved thin-walled molluscs occurs. Carbonate concretions up to 3 cm in diameter are scattered in the loess. The lowermost pedocomplex, PC10, consists of two paleosols separated by a carbonate crust up to 20 cm thick. Pale yellowish loess with carbonate concretions up to 8 cm diameter overlies PC10. PC9 consists of a dark brown/dark yellow brown, clayey to silty paleosol with a 40-cm-thick illuvial carbonate horizon at the base. This paleosol is covered by pale yellowish loess enriched with carbonate concretions in the upper part. PC8 consists of a brown, slightly carbonate-rich paleosol with an illuvial carbonate horizon of 40 cm thickness at the base. There is a continuous transition from paleosol PC8 to loess indicating that the loess/dust accumulation rate increased at the end of the interglacial. The loess between PC8 and PC7 is pale yellowish to gray and rich in carbonate. In the upper part of the loess the number of bioliths (interpreted as chambers of insects) increases toward the top. PC7 consists of a dark brown clayey paleosol with a B horizon characterized by slight clay illuviation. A compact carbonate horizon with relicts of bioliths underlies PC7. Upwards, the increasing loess content of the paleosol is indicated by a lighter, more yellowish color and a higher carbonate percentage. The following loess has a thickness of 11 m and is intercalated by layers of carbonate enrichment and a layer (100.00–103.00 m below surface) with bioliths.

PC6 consists of two brown paleosols. The lower one is of dark ochrous/brown color and enriched with secondary carbonate. At the bottom of this paleosol there is a carbonate crust. The upper dark ochrous/brown paleosol is more calcareous than the lower one. At the bottom there is an illuvial carbonate crust. The upper paleosol of PC6 is covered by pale yellowish loess containing carbonate concretions up to 20 cm diameter and bioliths at the top of the horizon.

PC5 is represented by a dark brown/reddish dark brown paleosol with Bt horizon rich in manganese and iron hydroxides and carbonate mycelium. The loess between PC5 and PC4 has a thickness of 11.40 m enriched in some intervals by carbonate concretions and bioliths. PC4 is represented by a dark brown/red brown paleosol with a few mottles of manganese and iron hydroxide. A 5 to 10 cm thick illuvial carbonate layer is at the bottom. The upper loess contains carbonate concretions up to 3 cm in diameter. PC3 consists of two paleosols. The lower paleosol is dark brown in the lower part and reddish dark brown in the upper part. It shows weak clay movements and minor manganese and iron hydroxide. Its illuvial carbonate horizon is weakly developed. The upper paleosol is represented by dark ochrous brown silt. The illuvial carbonate horizon is weakly developed with traces of bioliths. PC3 is covered by loess containing an enrichment of mollusc shells in the lower part (57.00 m). In the uppermost part of the loess bioliths are very common.

PC2 includes two paleosols separated by 1.80 m thickness of loess. The lowermost dark gray–brown paleosol is leached. Its illuvial carbonate horizon is represented by loose calcareous 0.80 m thick loess with bioliths. Above the 1.80-m-thick loess a second dark brown paleosol occurs being more calcareous than the lower one and containing many traces of pedofauna. The uppermost paleosol is covered by 17.00 m of thick pale yellowish loess rich in carbonate. The lower part of the loess cover is enriched with mollusc shells and bioliths. At a depth of 30.00 m carbonate concretions up to 10 cm in diameter occur indicating increased carbonate mobilization suggesting more moderate climatic conditions. Several horizons rich in small carbonate concretions up to 1.5 cm in diameter are intercalated in the loess.

PC1 consists of five paleosols and one intercalated loess layer. The lowermost dark brown paleosol is characterized by prismatic structure and leaching. In its 0.30 m thick carbonate horizon there are carbonate concretions

and crotovinas. Two dark-brown and two light-brown paleosols follow above being more calcareous and less structured than the lowermost paleosol of PC1. The youngest loess covering PC1 has a thickness of at least 19.50 m. The loess is intermingled by carbonate concretions and intercalated by several horizons of small carbonate concretions and bioliths, especially in the interval between 5.00 and 13.00 m below surface.

The grain-size spectra of the loess above PC1 are dominated by clay to medium silt (<20 µm) with an average percentage between 70 and 88% (Fig. 4). The high content of the grain-size fraction <20 µm indicates long-distant transport from the deserts to the west of the Afghan/Tadjic depression. The grain-size data indicate a slight increase in the clay content with depth for the loess above PC1. However, the grain-size spectra of 63–200 and 200–2000 µm are dominated by carbonate concretions. If compared with the average grain-size distribution of loess from the Middle Rhine Valley in Central Europe (Boenigk et al. 1994), the grain-size fraction <20 µm is much lower, less than 55%, than those from Darai Kalon/Chashmanigar. Additionally, the grain size >63 µm ranges between 15 and 30% in the Middle Rhine Area. A near distance transport from the flood plains of the rivers Rhine and Moselle is most likely for the aeolian sediments from the Rhine valley (Frechen et al. 1995).

The carbonate content ranges between 12 and 25% for the loess and the weak brown paleosols of the last intergla-

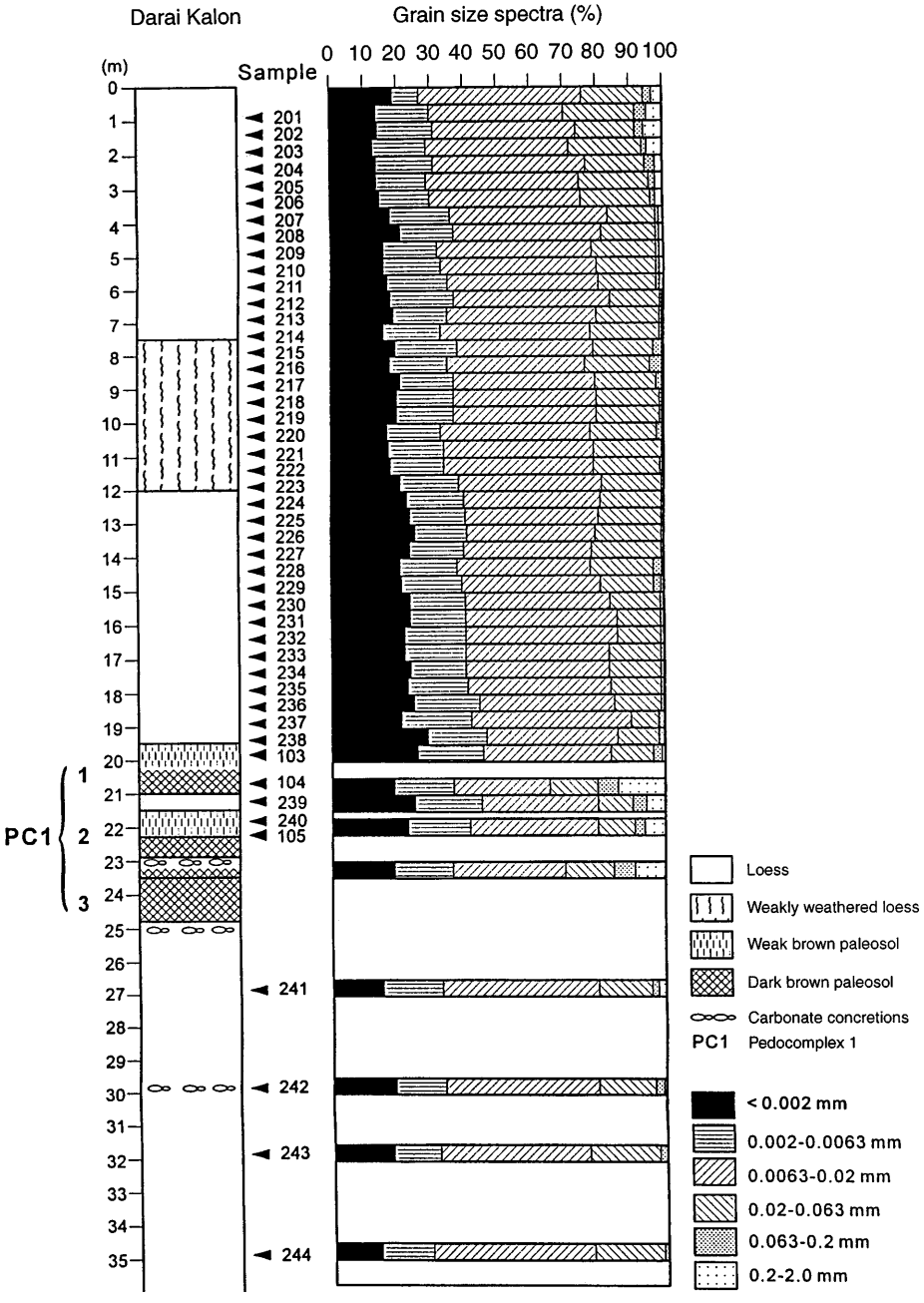

Fig. 4 Grain-size distribution for the loess above and below PC1. An increase of clay and fine silt grain size is observed with depth. The sand grain size is not related to quartz or feldspar minerals but to sand-sized carbonate concretions

cial/glacial deposits. Owing to secondary carbonate movement, it is not possible to use the carbonate content as an indicator for cold (loess) or warm (paleosol) climatic conditions. Bronger et al. (1995) described two Holocene soils on the Karatau range which were free of carbonate, indicating a high bicarbonate metabolism due to more humid climatic conditions. All paleosols were secondarily enriched with carbonates; hence, a differentiation between primary and secondary carbonates is important as described by Bronger et al. (1995).

A weak interstadial horizon is intercalated in the loess above PC1. The 4.50 m thick layer is rich in carbonate concretions. The uppermost last glacial loess and the Holocene soil are missing in the section at Darai Kalon.

Luminescence dating results

For the following discussion, the dosimetric results are listed in Table 1, and the paleodose values and ages are presented in Table 2. The average uranium and thorium contents are 2.74 and 9.83 ppm for the loess above PC1 and 2.31 and 9.35 ppm for the loess below PC5, respectively. The potassium content is constant with a mean value of 1.53 and ranging from 1.24 to 1.76 throughout the whole profile. The average total dose rate for the loess below PC5 is 3088 and 3188 µGy/years for IRSL and TL, respectively. The mean dose rate values are 3337 and 3520 µGy/years for the loess above PC1 for IRSL and TL,

Table 2 Paleodose values and loess deposition ages using IRSL and TL for both the regeneration and additive dose methods as described in the text

Sample	ISRL-REGEN paleodose (Gy)	IRSL-ADD paleodose (Gy)	TL-REGEN paleodose (Gy)	TL-ADD paleodose (Gy)	IRSL-REGEN age (in 1000 years)	IRSL-ADD age (in 1000 years)	TL-REGEN age (in 1000 years)	TL-ADD age (in 1000 years)
DRK201	56.8± 4.0	60.7± 2.5	66.9± 4.8	70.1± 2.5	19.3± 2.1	20.6± 1.9	21.9± 2.4	22.9± 2.0
DRK202	62.4± 5.3	60.0± 5.1	65.7± 5.4	61.9± 2.1	20.2± 2.3	19.4± 2.3	19.6± 2.3	18.4± 1.6
DRK203	67.3± 3.1	66.2± 6.1	66.4± 3.7	62.7± 1.8	22.5± 2.1	22.1± 2.7	20.6± 2.1	19.5± 1.7
DRK204	79.7± 2.5	76.9± 12.0	83.3± 2.6	76.1± 3.1	24.9± 2.2	24.0± 4.2	24.5± 2.2	22.4± 2.1
DRK205	73.1± 3.9	74.2± 7.6	71.2± 4.3	77.4± 3.9	21.6± 2.1	21.9± 2.8	21.2± 2.0	20.5± 1.8
DRK206	76.1± 2.6	77.6± 5.0	77.3± 3.1	76.0± 1.9	22.8± 2.0	23.3± 2.4	22.3± 2.0	21.9± 1.9
DRK207	70.8± 4.7	67.3± 12.3	67.8± 1.0	62.4± 2.6	20.8± 2.2	19.7± 3.9	20.0± 1.6	17.5± 1.6
DRK208	75.9± 2.8	72.4± 2.8	80.5± 1.6	79.4± 2.8	23.1± 2.0	22.0± 1.9	23.3± 1.9	23.0± 2.0
DRK209	80.8± 2.1	81.5± 5.3	84.9± 2.4	86.4± 3.5	24.8± 2.1	25.1± 2.1	24.4± 2.1	24.8± 2.3
DRK210	79.9± 6.2	78.3± 6.8	85.9± 5.8	86.4± 3.6	24.0± 2.7	23.6± 2.8	23.9± 2.5	24.0± 2.2
DRK211	85.8± 8.2	83.4± 14.1	99.2± 11.8	95.1± 5.3	25.6± 3.2	24.9± 4.7	27.5± 4.0	26.4± 2.6
DRK212	53.0± 2.3	90.9± 12.9	41.8± 1.6	62.2± 5.9	16.7± 1.5	28.6± 4.6	12.7± 4.6	18.9± 2.3
DRK213	90.5± 4.3	95.8± 7.6	88.3± 3.8	95.1± 3.3	28.0± 2.6	29.6± 3.3	26.6± 2.3	25.7± 2.3
DRK214	91.0± 2.3	98.1± 5.6	89.7± 4.2	93.2± 3.9	28.4± 2.4	30.6± 3.0	25.6± 2.4	26.6± 2.5
DRK215	110.9± 2.3	120.8± 11.7	106.2± 10.4	118.7± 4.1	34.4± 2.8	37.5± 4.7	30.3± 3.9	33.9± 3.0
DRK216	111.9± 4.2	97.8± 9.8	111.6± 4.0	101.4± 5.3	36.1± 3.2	31.6± 4.0	36.0± 3.1	32.7± 3.1
DRK217	113.6± 4.4	121.4± 9.1	116.2± 4.7	120.9± 3.2	34.4± 3.1	36.7± 4.0	32.2± 3.0	33.5± 2.9
DRK218	104.4± 4.9	122.3± 5.9	100.0± 3.4	118.1± 6.9	32.9± 3.1	38.6± 3.6	28.9± 2.6	34.2± 3.5
DRK219	109.1± 6.9	136.5± 70.3	103.1± 5.0	127.9±15.7	30.1± 3.2	37.4± 3.4	30.2± 2.9	37.4± 5.5
DRK220	121.2± 4.7	115.2± 14.4	121.5± 4.9	109.7± 4.9	38.6± 3.4	36.7± 5.4	35.5± 3.2	32.0± 3.0
DRK221	116.1± 4.9	105.8± 13.3	121.2± 3.9	113.2± 3.0	34.6± 3.1	31.5± 4.7	34.2± 3.0	32.0± 2.8
DRK222	139.6± 7.6	160.7± 7.1	128.6± 2.1	152.5± 4.3	42.2± 4.1	48.6± 4.4	36.3± 3.0	43.1± 3.7
DRK223	121.4± 7.1	133.1± 43.6	125.9± 6.9	136.0± 4.1	35.6± 3.6	39.1±13.2	34.3± 3.4	37.1± 3.3
DRK223								
DRK225	136.0± 5.4	150.8± 11.9	133.2± 3.4	144.6± 2.5	41.3± 3.7	45.8± 5.1	39.5± 3.3	42.9± 3.5
DRK226	147.7± 12.6	169.0± 14.6	151.6± 7.1	167.2± 2.6	44.0± 5.2	50.4± 6.0	41.9± 4.0	46.2± 3.9
DRK227	153.7± 4.2	157.3± 8.6	154.5± 2.8	174.7± 3.9	47.5± 4.0	48.6± 4.7	45.1± 3.8	51.0± 4.3
DRK228	124.1± 23.4	108.7± 16.9	135.7± 14.6	126.1± 7.0	39.9± 8.2	35.0± 6.1	41.4± 5.6	38.5± 3.8
DRK229	148.2± 5.0	155.4± 6.3	158.9± 3.1	161.1± 5.3	48.3± 4.2	50.7± 4.6	48.5± 4.1	49.2± 4.4
DRK230	170.1± 7.8	167.0± 8.3	188.1± 5.8	181.5± 3.5	55.4± 5.1	54.4± 5.1	58.7± 5.1	56.6± 4.7
DRK231	171.4± 4.8	172.7± 8.9	180.4± 4.8	189.7±3.3	51.4± 4.4	51.8± 4.9	55.2± 4.6	52.5± 4.5
DRK232	194.2± 11.5	175.0± 19.7	194.2± 8.1	190.8±2.8	57.7± 5.8	52.0± 7.2	53.3± 4.9	52.3± 4.4
DRK233	190.4± 5.5	175.6± 13.9	226.4± 1.8	208.5±2.6	53.7± 4.6	49.5± 5.6	59.8± 5.0	55.0± 4.6
DRK234	199.0± 5.7	217.0± 13.0	202.8± 5.2	230.0±3.3	54.5± 4.7	59.3± 6.0	55.4± 4.7	62.8± 5.2
DRK235	202.7± 8.7	246.6± 75.5	220.8± 7.6	306.1±2.9	53.8± 4.9	65.4±20.7	56.1± 5.0	77.7± 6.4
DRK236	66.8± 1.8	133.2± 5.3	73.7± 2.2	144.0±2.5				
DRK237	205.8± 4.0	270.2± 24.6	210.1± 4.4	271.5±2.2	50.5± 4.2	66.3± 8.1	49.7± 4.2	64.2± 5.3
DRK238	232.1± 11.9	257.6± 13.3	236.1± 9.9	253.2±2.4	55.6± 5.3	61.6± 5.9	54.0± 5.0	57.9± 4.8
DRK239	217.0± 8.6	223.8± 12.5	225.5± 9.0	253.4±2.0	67.0± 6.1	69.1± 6.8	65.8± 6.1	73.9± 6.2
DRK240	228.6± 13.5	311.5± 40.3	241.7± 10.6	369.8±4.5	66.3± 6.6	90.3±13.8	67.4± 6.2	103.1± 8.5

For continuation of Table 2 please see the next page

Table 2 (Continued)

Sample	ISRL-REGEN paleodose (Gy)	IRSL-ADD paleodose (Gy)	TL-REGEN paleodose (Gy)	TL-ADD paleodose (Gy)	IRSL-REGEN age (in 1000 years)	IRSL-ADD age (in 1000 years)	TL-REGEN age (in 1000 years)	TL-ADD age (in 1000 years)
DRK241	300.3± 26.0	299.3± 78.2	346.0± 15.5	394.1± 4.6	93.9±11.1	93.6±25.6	102.7± 9.8	117.0± 9.8
DRK242	300.6± 8.3	389.2± 231.7	343.0± 9.9	500.8± 9.3	94.1± 8.0	93.7±25.6	102.1± 8.9	149.0±12.5
DRK243	305.4± 20.2	307.3± 19.9	311.8± 21.1	383.6±14.9	98.6±10.2	99.2±10.2	94.1±10.0	115.7±12.5
DRK244	388.1± 22.3	432.3± 51.1	404.8± 26.1	522.4± 8.0	112.1±11.1	125.1±17.9	111.4±11.7	143.8±12.0
DRK245	302.3± 19.5	354.5± 40.5	350.0± 12.0	416.6± 7.1	91.3± 9.4	107.1±14.9	102.4± 9.0	121.9±10.0
DRK246	379.7± 9.6	434.1± 20.7	428.9± 8.6	612.6± 4.8	103.1± 8.8	117.8±11.1	109.6± 9.4	156.6±13.1
DRK247	435.5± 13.0	414.1± 52.2	441.8± 9.6	540.1± 7.4	122.9±10.6	116.8±17.5	119.5±10.2	146.1±12.2
DRK248	403.6± 14.8	493.0± 273.4	467.3± 11.4	789.7±14.6	124.4±11.0	158.8±15.1	135.6±11.6	229.2±19.3
DRK249	346.3± 24.7	444.3± 70.5	445.0± 27.9	622.8±15.9	112.9± 9.5	146.6±13.8	130.6±13.6	182.8±15.8
DRK250	378.4± 19.0	467.3± 48.1	489.8± 31.1	688.6± 3.7	115.7±10.9	142.9±18.6	144.4±14.8	205.0±16.5
DRK251	334.0± 28.0	379.8± 66.6	408.3± 34.2	491.6±12.5	117.4±13.5	133.5±25.7	137.3±15.9	165.3±13.8
DRK252	392.4± 31.6	434.3± 46.6	531.3± 26.4	719.7± 7.4	122.5±13.9	135.6±18.2	163.0±15.5	220.8±18.0
DRK253	459.2± 34.3	566.0± 41.3	575.7± 25.7	827.4± 6.4	143.3±15.7	176.6±19.2	177.2±16.4	254.6±20.7
DRK254	445.5± 32.2	536.9±133.9	589.1± 25.2	822.7±11.6	145.0±15.6	176.5±16.4	183.2±16.9	255.9±21.2
DRK255	471.9± 23.8	557.3± 34.8	596.3± 17.4	897.6± 5.6	126.5±12.1	149.4±15.3	156.2±13.6	235.1±19.3
DRK256	456.2± 36.3	478.0± 81.5	800.9± 33.4	911.3±15.2	146.7±16.6	161.1±15.3	249.2±22.8	283.6±23.6
DRK257	463.6± 31.4	548.2± 43.3	606.9± 32.9	808.0±13.8	145.3±15.3	171.8±19.4	184.2±18.1	245.3±20.5
DRK258	453.8± 23.9	575.6±182.0	689.7± 42.3	552.6±17.3	142.1±13.7	180.6±17.6	209.2±21.4	167.6±14.6
DRK259								
DRK260	476.1± 56.3	541.5± 32.8	710.5± 70.6	737.4±7.0	151.2±21.6	172.0±17.3	224.2±28.6	232.6±18.8
DRK261	509.7± 18.2	473.4±186.6	614.9± 25.8	769.9± 6.1	167.2±14.8	162.8±17.2	195.0±17.9	244.1±20.1
DRK262	354.7± 24.3	321.0±117.3	435.7± 12.8	552.8± 3.4				
DRK263	570.9± 59.3	890.9±499.1	798.4±117.1	1331.5±23.3	161.6±21.0	251.0±21.6	217.1±36.1	362.0±29.2
DRK264	445.5± 27.8	589.3±288.8	600.8± 12.8	982.4±40.0	139.9±14.3	183.7±18.8	189.3±15.8	309.6±28.0
DRK265	487.4± 37.6	628.3±151.1	840.6± 85.4	1202.0±30.8	170.9±14.1	224.3±20.1	302.0±38.9	431.9±36.0
DRK266	458.0± 39.1	519.9±159.3	773.1± 24.5	725.8±31.6	159.7±13.3	187.2±18.8	273.0±23.3	256.3±23.1
DRK267								
DRK268	522.6± 31.1	834.7±192.4	968.9± 79.2	1333.1±46.9	171.9±17.2	279.9±27.2	304.8±35.3	419.4±37.3
DRK268b	419.5± 21.1	475.1±104.0	598.2± 37.2	676.6±19.6				170.9±15.0
DRK269	411.9± 36.4	379.8± 60.0	724.6± 97.4	578.7±15.8	133.4±16.0	123.0±21.8	214.0±33.9	
DRK270	540.4± 17.8	672.8±330.6	891.3± 44.7	1198.2±27.7	172.4±14.8	207.5±18.4	286.3±26.9	384.3±31.8
DRK271	519.7± 36.6	–	776.1± 42.5	1061.3± 6.7	164.2±17.6	217.6±29.6	236.1±23.3	322.9±26.5
DRK272	371.6± 7.0	302.5± 63.8	748.7±124.5	497.7±27.9	126.8±10.7	101.3± 9.9	233.5±43.4	155.2±15.5
DRK273	605.4±107.7	728.9±288.7	769.8±144.5	1006.8±31.6	175.6±34.3	203.0±19.8	212.1±43.5	277.3±24.5
DRK274	424.3± 13.7	–	784.8± 37.2	643.5±10.0	157.9±13.7	166.5±20.0	277.0±26.3	227.2±19.0

respectively. The IRSL dose rate is smaller due to a lower alpha efficiency for IRSL. Uranium and thorium contents decrease with depth, resulting in a decrease of the average total dose rate. The dose rate values are of the order of 3500–5500 µGy/year and are comparable with those from other European loess regions (Frechen 1991; Frechen et al., in press).

The IRSL data show an increase of paleodose with depth down to PC2 for both the regeneration and additive dose methods. Below PC2 there is still a general slight increase of paleodose with depth as demonstrated in Table 2. However, for samples taken from below PC5 the paleodose data are extremely scattered from sample to sample, resulting in paleodose values of 500±150 Gy for IRSL-REGEN and 600±300 Gy for IRSL-ADD. Such a scattering is not dose dependent and is not acceptable for dating; hence, IRSL dating methods are not applicable for the older samples. A correction model cannot be applied because of the sample-to-sample scattering.

The TL-REGEN paleodose determinations indicate an increase of paleodose with depth down to PC6 resulting in values of 800±200 Gy for TL-REGEN (excluding one data point; DRK236, probably mistaken during preparation). The data set for the TL additive dose method looks similar, resulting in an increase of paleodose up to 1330 Gy. However, the paleodose data show an extreme scattering for the loess below PC5, which does not allow a reliable and meaningful correction of the underestimated TL age results. The paleodose values range within 1000±300 Gy below PC5. If the paleodose and age values are compared with the geologically and stratigraphically estimated ages, an underestimation of more than 50% is likely for the lowermost sample.

The highest IRSL paleodose values are approximately 600 and 900 Gy for the regeneration and additive dose methods, respectively. The lowest IRSL paleodose values are between 50 and 60 Gy for both applied techniques. The highest TL paleodose values are approximately 970 and 1330 Gy for the regeneration and additive dose methods, respectively.

The IRSL paleodose determinations are systematically lower than those by TL despite being obtained on identical

samples. A mean IRSL age and paleodose underestimation of less than 5% is determined for the loess above PC1 for both the additive dose and regeneration methods. The difference between IRSL and TL increases with depth up to 30–40% for samples taken from below PC5. It is important to note that TL and IRSL age estimates are not to be regarded as "absolute dates" below PC1! The criteria for assessing an IRSL and TL age underestimation of the loess below PC1 is based on the application of a correction model based on the presence of the B/M boundary and a lifetime of the electron traps of 300 000 or 400 000 years (M. Frechen, unpublished data).

The lowermost sample (DRK274) was taken from pale yellowish loess intermingled with carbonate concretions up to 5 cm in diameter between PC10 and PC9, approximately 1 m below the carbonate horizon of PC9. Indepen-

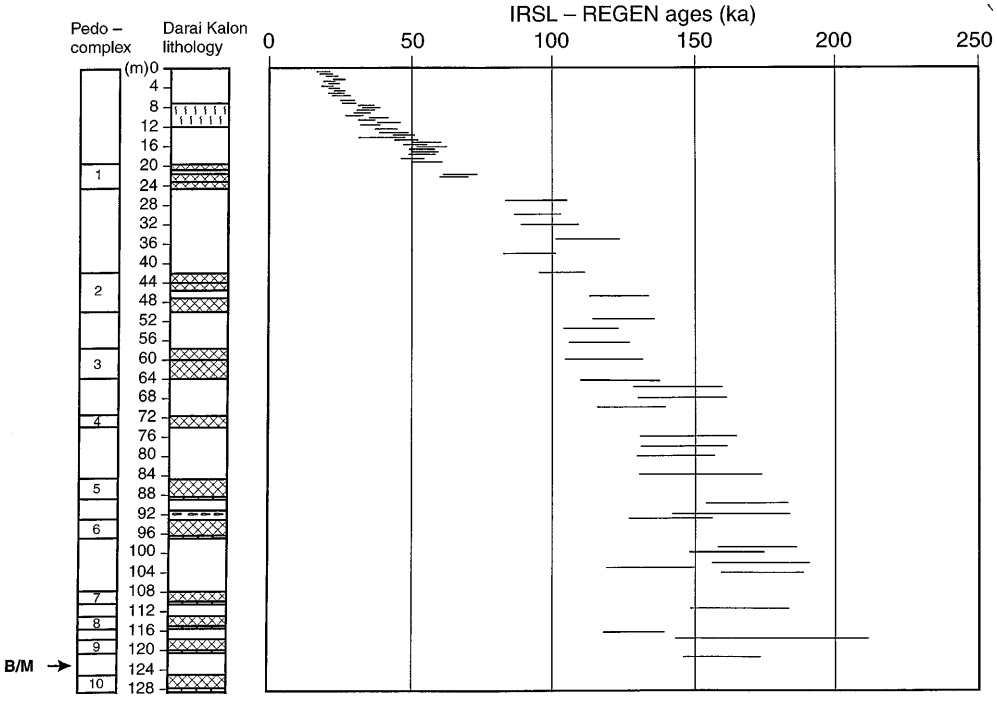

Fig. 5 Infrared stimulated luminescence (IRSL) dating results with depth using the regeneration method for samples from the section at Darai Kalon

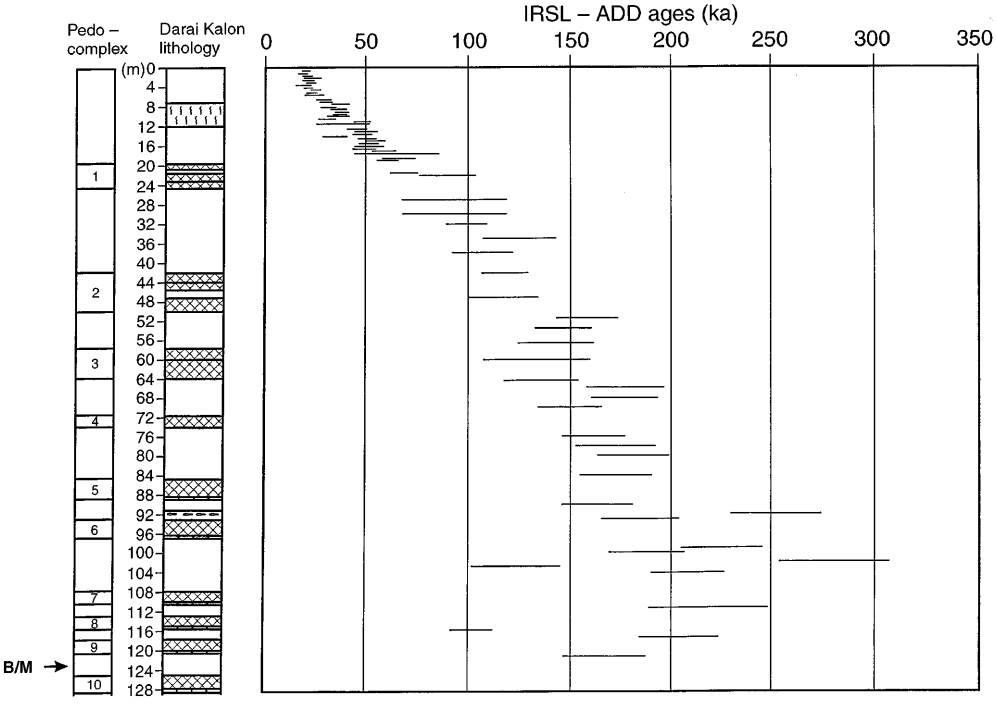

Fig. 6 IRSL dating results with depth using the additive dose method from the section at Darai Kalon

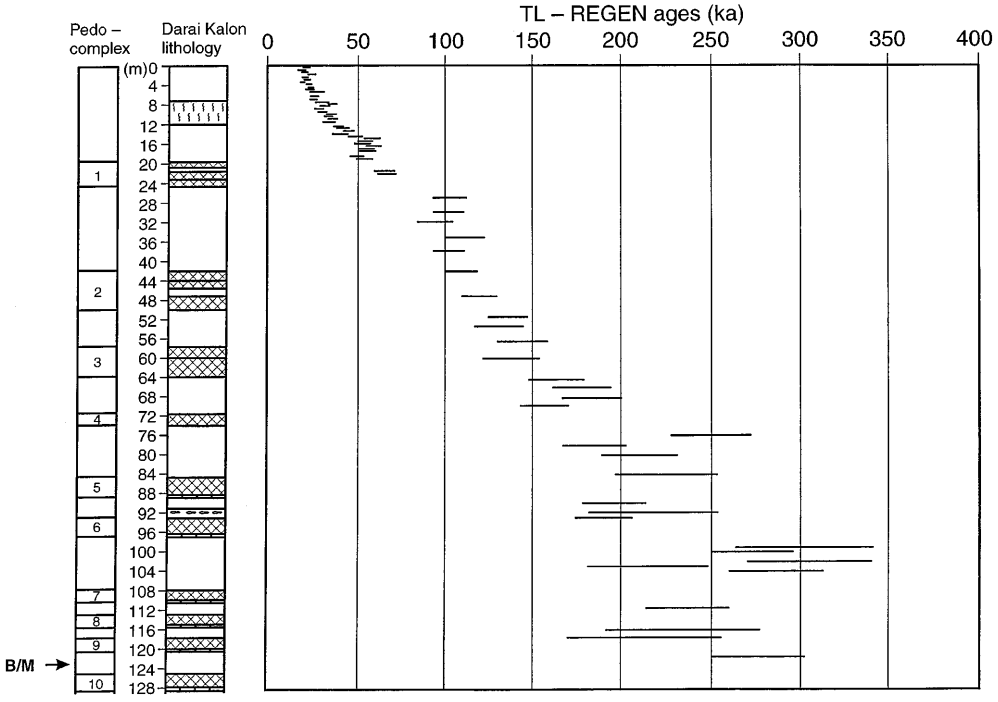

Fig. 7 Thermoluminescence (TL) dating results with depth using the regeneration method for the section at Darai Kalon

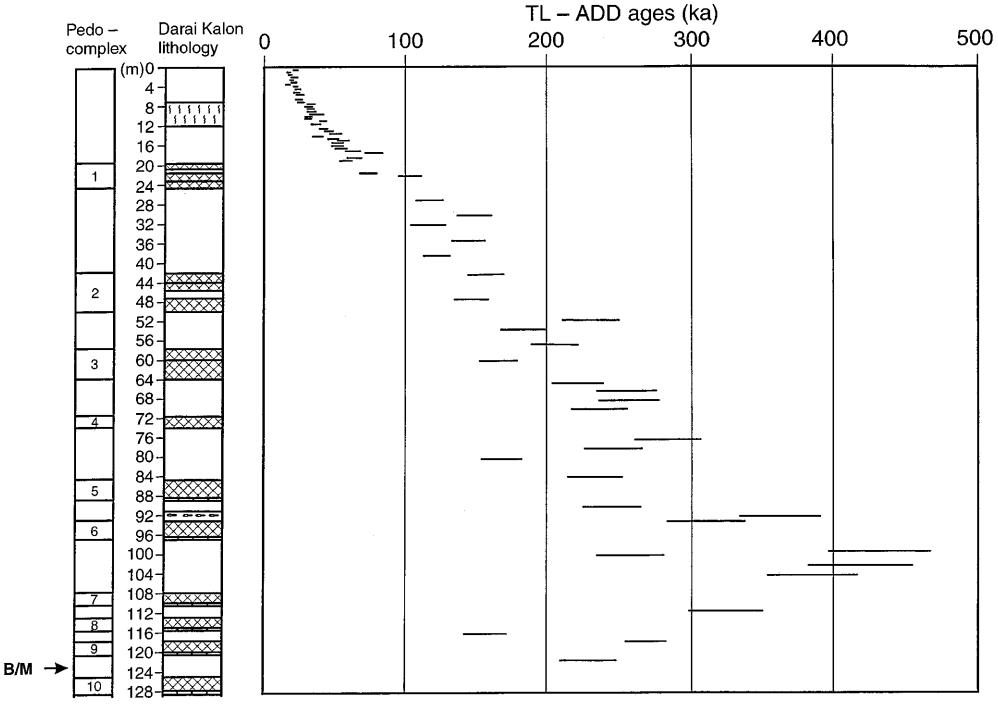

Fig. 8 Thermoluminescence dating results with depth using the additive dose method for the section at Darai Kalon

dent age control is provided by the presence of the B/M boundary between PC10 and PC9, for which an age of 788 000±1800 years was calculated elsewhere (Tauxe et al. 1996). The TL and IRSL determinations yielded TL age results between 230 000 and 280 000 years and IRSL age results between 160 000 and 170 000 years, indicating a significant age underestimation for all applied methods, if compared with the independent data of the B/M boundary.

The samples taken between PC9 and PC5 (DRK273-261) from pale yellowish loess range in age between 431 900±36 000 and 155 200±15 500 years for TL-ADD and between 304 800±35 200 and 189 300±15 800 years for TL-REGEN. However, they do not indicate a continuous age increase with depth from sample to sample. The apparent IRSL age estimates are between 279 900±27 200 and 101 300±9900 years. The data sets are not stratigraphically

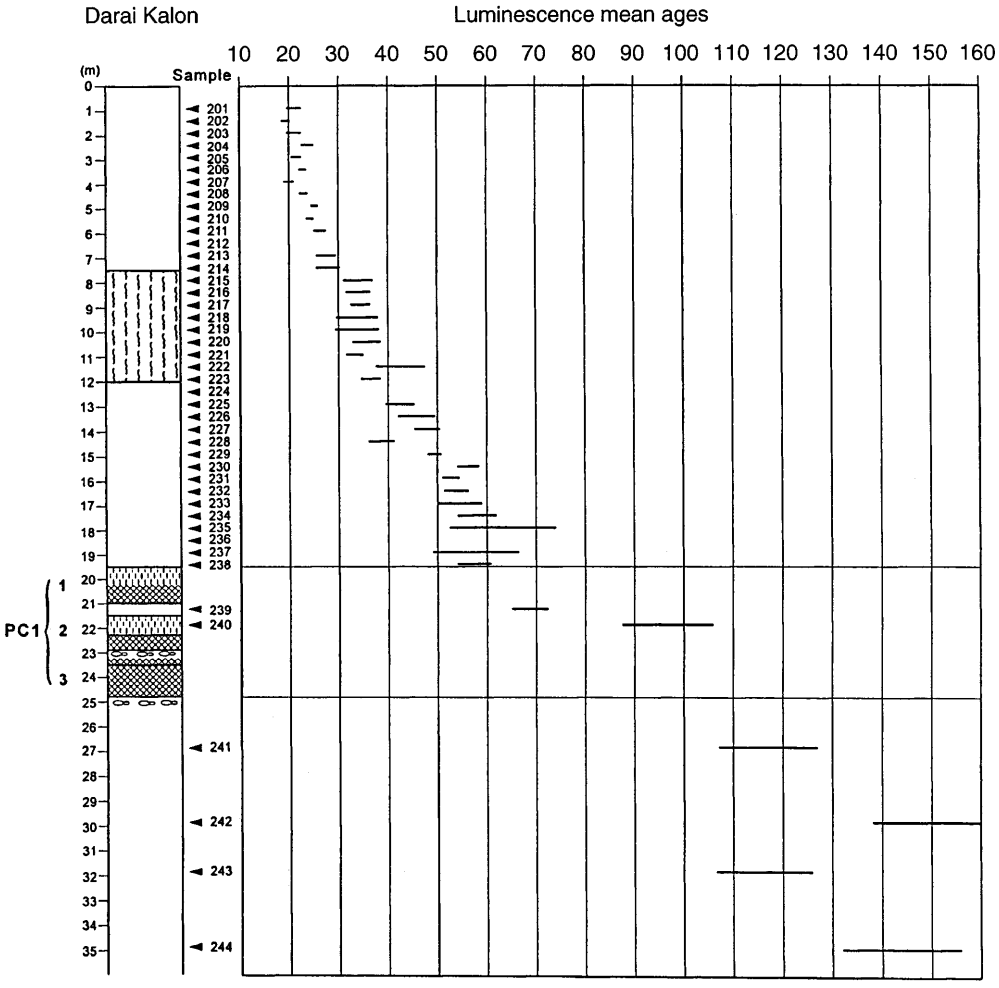

Fig. 9 Mean luminescence age values based on the age of determinations by IRSL and TL using both the additive dose and regeneration methods for the last interglacial/glacial cycle

consistent. However, if statistically analyzed, a slight increase of the age data with depth is indicated and a correction of the smoothed data set could therefore be applied (M. Frechen, unpublished data).

The samples (DRK260-241) taken between PC5 and PC1 from loess indicate a better IRSL and TL age increase with depth than those from between PC9 and PC5, if the whole data set is analyzed (Figs. 5–8). The IRSL ages range from 146700±16600 and 180600±17600 years above PC5 to 91300±9400 and 93600±25600 years below PC1 for the regeneration and additive dose methods, respectively. The TL ages are approximately 20% higher indicating age estimates ranging from 249200±22800 and 283600±23600 years to 94100±10000 and 115700±12500 years for the regeneration and additive dose methods. As the data sets indicate a significant age underestimation, accumulation rates cannot be calculated.

The samples taken from PC1 (DRK240 and 239) and above PC1 (DRK238-201) are in excellent stratigraphic order and show a paleodose and age increase with depth (Fig. 9). Furthermore, there is very good agreement between IRSL and TL data up to 110000 years, which is in contrast to what is known from Central and Southeast Europe (Frechen et al., in press). PC1 consists of three dark-brown and two light-brown paleosols rich in secondary carbonate. The whole pedocomplex has a thickness of 5.25 m. Sample DRK240 was collected from the light-brown paleosol between the upper and middle dark-brown paleosol of PC1, at 22 m depth. Sample DRK239 was taken from loess intercalated between the middle and uppermost dark-brown paleosols at 21.25 m depth. The luminescence age estimates range between 90300±13800 (DRK240) and 66300±6600 (DRK239) years for IRSL and 103100±8500 (DRK240) and 65800±6100 (DRK239) years for TL.

Discussion of methodological aspects

Upper dating limit

The upper dating limit is controlled by several parameters which vary significantly from mineral to mineral and from sample to sample. The most important controlling effects are defined as the stability and the saturation of the luminescence signal, which depends on the dose rate of the sediment (Aitken 1985; Mejdahl 1989). The IRSL and TL paleodose values show an increase with depth for both the regeneration and the additive dose methods. The TL-ADD

paleodose values range between 60 and 1350 Gy. As demonstrated in Figs. 5–8, IRSL and TL age values increase linearly with depth down to PC1. There is little difference between the individual methods. The IRSL and TL paleodose results are within the 1-sigma standard deviation for both IRSL and TL additive dose and regeneration methods. However, paleodose determinations below PC1 indicate a systematic difference with depths between the individual methods. The average paleodose value for IRSL-REGEN and IRSL-ADD is approximately 3 and 4.2% less than those of TL-REGEN and TL-ADD for the samples above PC1 (DRK201-240), respectively. Between PC1 and PC5 (samples DRK241-260) the difference between the paleodose values increases, indicating an average underestimation of IRSL-REGEN and IRSL-ADD of 20.6 and 18.6%, respectively, if compared with TL. The paleodose determinations for the samples below PC5 (DRK261-274) indicate an underestimation of IRSL-REGEN and IRSL-ADD of 36.0 and 38.7%, respectively, when compared with TL. The underestimation of IRSL is most likely not caused by insufficient bleaching of the sediment prior to deposition, as demonstrated for the loess above PC1. The statistical trend indicates a slight increase of paleodose with depth. If the average age values for TL-ADD are calculated for each loess unit, e.g., loess between PC1 and PC2, etc., a relative slight increase with depth is determinable. However, the resolution of the data set and the increase with depth are too low to distinguish relatively between the single interglacial/glacial cycles below PC5.

The highest paleodose was obtained for sample DRK265, collected between PC7 and PC8. The ED values of 1202 and 1333 Gy, obtained by the additive dose TL method, result in apparent ages over 400 000 years (Table 2). However, the EDs determined by the regeneration method show lower values, indicating an upper limit between 900 and 1000 Gy. It should be pointed out that those luminescence ages with a paleodose above 500–600 Gy depend entirely on the dose rate of the sediment. Lower dose rates will result in older age limits. The model of long-term loss of luminescence centers (Debenham 1985; Wintle 1985), for which a value close to 150 000 years was suggested, seems to be underestimated. Despite the model proposed by Debenham (1985), a correction model needs to be paleodose- and dose-rate dependent as described by Musson and Wintle (1994). They clearly pointed out that their correction model only takes into account a simple time-dependent behavior, which needs to be modified to include the effect of variable dose rates from sample to sample and site to site, as proposed by Mejdahl (1988, 1989). Investigations of luminescence properties of loess from below the B/M boundary indicate an upper numerical age limit as well as paleodose- and dose-rate dependence (!) in the range of 250 000–400 000 years, as determined for loess from Moravia, Hungary, Tadjikistan, and China (Frechen and Zhou 1995; M. Frechen, unpublished data). Older age estimates could be possible if the dose rate is significantly lower than those found in the current study of the Tadjic loess. However, a correction model (sensu Wintle 1990) does not seem to improve the dating results significantly for loess from below the PC1, designated to be older than 130 000 years. If the data set is interpreted in detail, a significant scattering from sample to sample is found for those samples with a paleodose larger than 600 Gy (Table 2). Additionally, the ED increase with depth is very low for samples from below PC1 and especially from below PC2, indicating either a very high accumulation rate or a paleodose value near saturation.

The IRSL/REGEN ages show a linear increase with depth down to PC1 (Fig. 5). Below PC1 there is still an increase with depth, but the age values are systematically and significantly underestimated resulting in upper IRSL-REGEN ages between 150 000 and 200 000 years for the loess above the B/M boundary, for which an independent age of 788 000±1800 ka (Tauxe et al. 1996) is assumed. Reliable dating for the loess below PC1 is not available with IRSL using the regeneration technique. Even the application of a correction model using a lifetime of 150 000 years does not improve the data set because of the standard deviation and scattering from sample to sample.

The IRSL age determinations using the additive dose methods indicate an age increase with depth down to PC5. The age results are in the range of 200 000 to 250 000 years for the loess above the B/M boundary, indicating a significant age underestimation of more than 60% for the loess below PC5 using the IRSL additive dose method. The IRSL-ADD ages show an increased scattering below PC5 (Fig. 6). The TL/REGEN ages increase with depth at least down to PC5 (Fig. 7) resulting in TL-REGEN age estimates ranging between 250 000 and 300 000 years for the loess directly above the B/M boundary. The same significant underestimation is obtained for the TL regeneration method. TL-ADD ages increase with depth down to at least PC5 (Fig. 8). These age results are in agreement with geological estimates for the last and penultimate glacial loess. However, there is again an extended scattering of age estimates and paleodose values from sample to sample, most likely due to near-saturation conditions. The stratigraphically oldest sample yielded TL ages ranging between 200 000 and 250 000 years. However, the chronologically oldest sample is DRK268 with a TL age older than 400 000 years. A simple correction model by applying a lifetime of 400 000 years does not improve the data set below PC2 because of the low resolution due to the 1-sigma standard deviation of 8–15% combined with significant scattering from sample to sample and little increase of paleodose with depth. If statistical methods are applied, a correction model could be determined by using a trend analysis (M. Frechen, unpublished data). An application of such a model appears to be successful for the section at Darai Kalon/Chashmanigar where a more-or-less continuous loess record is available. However, a general application to other loess areas does not work unless a basically continuous record and independent dating are available in order to correct IRSL and TL dating results.

Sensitivity change after bleaching

If the results for the additive dose and regeneration methods, as applied for the paleodose estimates of last glacial loess, are compared, little difference is observed for both IRSL and TL. The uppermost 40 samples, spanning PC1 and the loess above PC1, indicate sensitivity changes of the order of 4.6 and 6.8% for IRSL and TL, respectively. The loess between PC1 and PC5 indicates average sensitivity changes of 13.6 and 22.2% for IRSL and TL, respectively. Finally, the loess below PC 5 indicates sensitivity changes of the order of 14.6 and 18.1% for IRSL and TL, respectively.

The sensitivity changes observed in IRSL and TL results of the last and penultimate loess are similar to results from the Middle Rhine area (Frechen 1992; Frechen et al. 1995).

Underestimation of IRSL

The TL and IRSL paleodose estimates show stratigraphically consistent behavior and are in agreement for the loess above PC1. This is in contrast to results applying combined IRSL and TL dating on loess and reworked loess from Europe (Frechen et al. 1995; Frechen et al., in press) where tephra horizons provided independent age

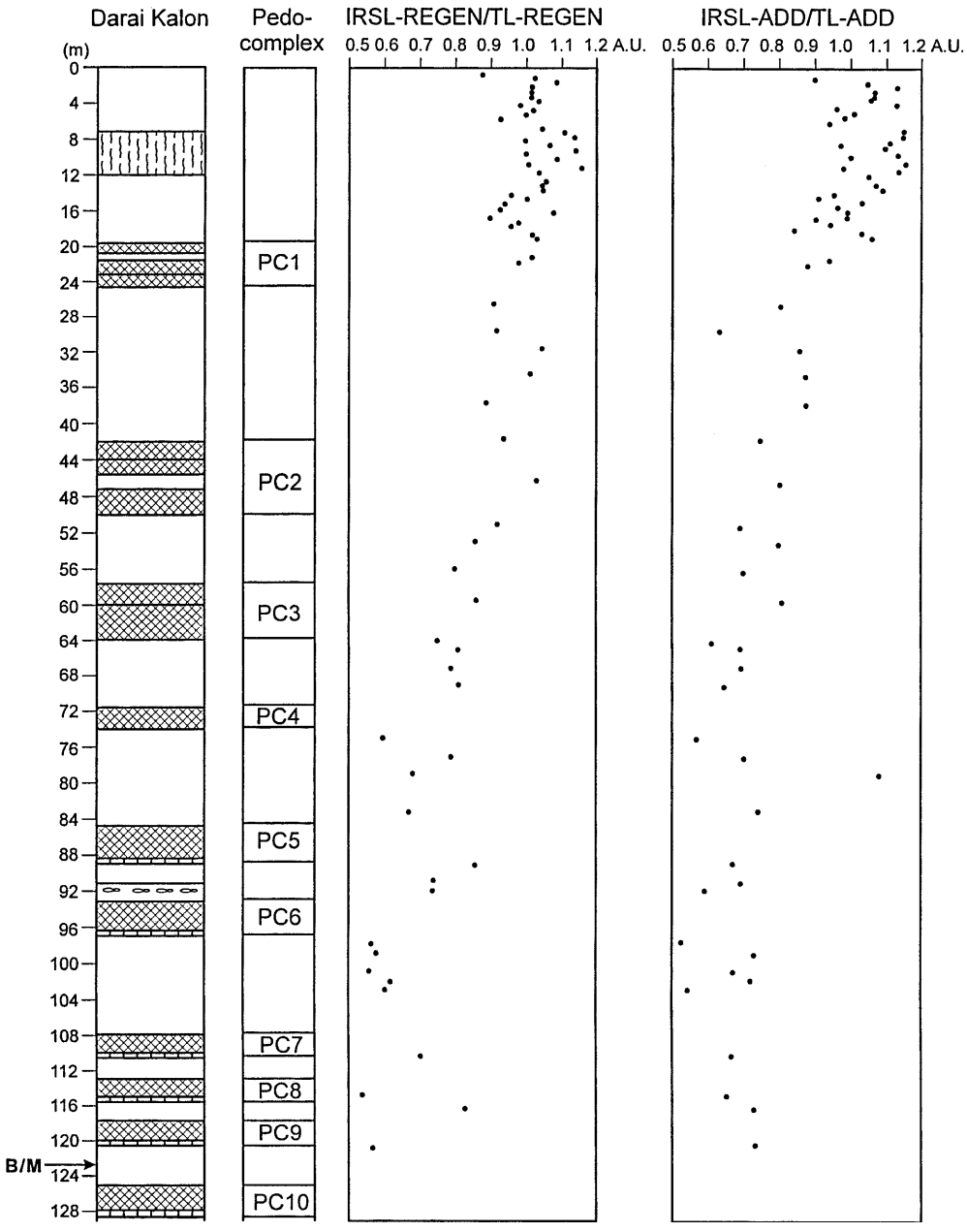

Fig. 10 Underestimation of IRSL with depth using the paleodose ratio of IRSL/TL

control. In Europe loess or loess-like deposits show often an unsystematic difference between TL and IRSL results. The IRSL ages are often in agreement with the geological estimates and increase with depth, whereas TL age estimates scatter unsystematically due to insufficient bleaching or reset of the radiometric clock prior to deposition. The loess or loess-like sediments along extended river valleys, such as the Danube or Rhine in Europe, derive, to a great extent, from the river floodplains. Hence, a short-distance transport for most of the Central European loess regions is most likely, which is in contrast to the Central Asian loess area. The similar behavior of IRSL and TL measured in the last glacial loess at Darai Kalon/Chashmanigar clearly indicates a long-distance transport. Thus, the aeolian dust which formed the last glacial loess was well bleached prior to deposition, and the radiometric clock was completely reset for both TL and IRSL dating methods. The slight underestimation of IRSL between 3 and 4.2% in the loess above PC1 could be due to laboratory illumination as described previously (Frechen et al., in press). If the ratios IRSL-REGEN/TL-REGEN and IRSL-ADD/TL-ADD are plotted against depth, a systematic decrease of both ratios with depth is found (Fig. 10). The data set concerning the regeneration method indicates a transition from a ratio approximately 1.0–0.7 between PC2 and PC4. This average ratio then remains stable down to the lowermost sample above PC10. The data set concerning the additive dose method shows consistent behavior for the ratios below PC1, indicating an average ED ratio between 0.6 and 0.7. The difference could be explained by the different stability and lifetime of luminescence centers (M. Frechen, unpublished data).

Chronostratigraphic aspects

The luminescence age estimates need to be discussed in four age groups from the youngest to the oldest:

1. Loess above PC1
2. Sediments of PC1
3. Loess between PC1 and PC5
4. Loess below PC5

Loess above PC1

The sediment between PC1 and the surface of the profile consists of typical pale yellowish loess intercalated by several horizons rich in small carbonate concretions. These layers are interpreted as representing periods of more intense weathering. Between the surface and PC1, samples were collected every 0.50 m for this study. A higher-resolution study of the last and penultimate glacial loess is in preparation and will provide data points every 0.25 and 0.50 m for the last glacial and penultimate glacial loess, respectively (M. Frechen et al., in preparation).

All applied dating methods and techniques are in agreement, indicating age estimates between 19300±2100 and 57700±5800 years for IRSL-REGEN; 19400±2300 and 66300±8100 years for IRSL-ADD; 19600±2300 and 59800±5000 for TL-REGEN; and 18400±1600 and 77700±6400 years for TL-ADD. All results are in excellent agreement with the geological estimates for the age of loess above PC1, if compared with the marine oxygen-isotope record. If PC1 is interpreted as last interglacial and early glacial, OIS 5, the loess above the first pedocomplex is interpreted as OIS4 to OIS2, as demonstrated by the luminescence age data sets. The combined IRSL and TL dating study of the loess above PC1 indicates a basically continuous accumulation of loess (dust) between 20000 and 70000 years before present. However, the high-resolution dating is not sensitive enough to distinguish, for example, hiatuses indicated by small layers of carbonate concretions due to increased weathering or erosion. The uppermost loess, younger than 20000 years, is missing from the record at Darai Kalon. By applying combined IRSL and TL dating for the loess above PC1, the loess accumulation rate can be calculated more accurately. The uppermost 6 m were deposited between 20000 and 25000 years, resulting in a continuous accumulation rate of 1.20 m/1000 years (Fig. 11). The loess between 6.00 and 11.50 m below the surface was deposited between 28000 and 35000 years, resulting in an accumulation rate of 0.78 m/1000 years for this part of the section. The 4.50-m-thick interstadial horizon, intercalated in the loess above PC1, is most likely an equivalent of oxygen-isotope stage 3, as demonstrated by the luminescence age estimates (Fig. 9). The loess between 11.50 and 19.50 below the surface was deposited between 35000 and 65000 years, resulting in an accumulation rate of 0.27 m/1000 years. PC1 has a total thickness of 5.75 m at the section at Darai Kalon, resulting in an average loess or sediment accumulation rate of 0.10 m/1000 years, if we take into consideration a pedosedimentary model for PC formation in general. All presented accumulation rates are regarded as mini-

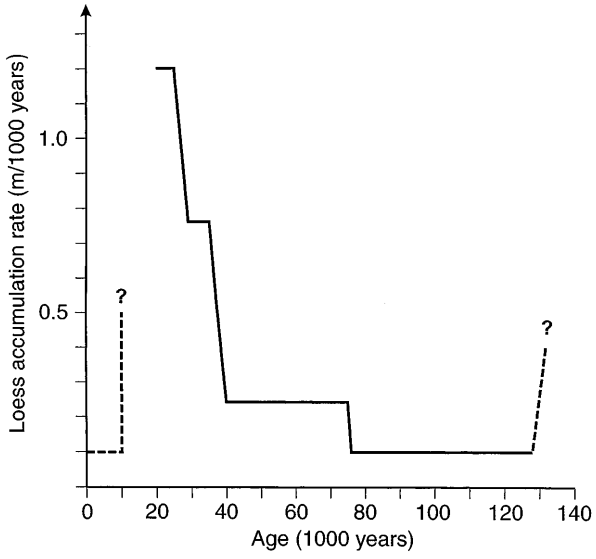

Fig. 11 Loess/dust accumulation rates for the last interglacial/glacial cycle based on thickness and luminescence data

mum values. No correction for loess compaction for the lower part of the last glacial loess and PC1 was applied in this study. However, the accumulation rates interpolated for the last glacial loess in this study are far higher than those of 0.045 m/1000 years reported by Shackleton et al. (1995) for the section at Karamaydan. No dating control was available for the last glacial loess at the section at Karamaydan, except the record of magnetic susceptibility, which is insufficient as a chronological dating tool. An independent reliable chronological counter-control of the terrestrial record (here: the loess record) is always required in order to extrapolate accumulation rates or to correlate the marine and terrestrial record in detail. The loess accumulation rate for the section at Karamaydan seems to be low according to the model of Shackleton et al. (1995) and is regarded to be anomalous as pointed out by the same authors because of the small thickness of the loess horizon at the top of the section. It is probable that the described section from Karamaydan (Foerster and Heller 1994) does not include the complete last glacial record.

The data set of this study fits very well with the record of dust accumulation as extrapolated from a theoretical ice-volume model as proposed by the SPECMAP record (Shackleton et al. 1995). The maximum dust or loess accumulation rate for the section at Darai Kalon was associated with increased ice volume at least during the last interglacial/glacial cycle (Fig. 11); thus, the two records are comparable for the past 130 000 years.

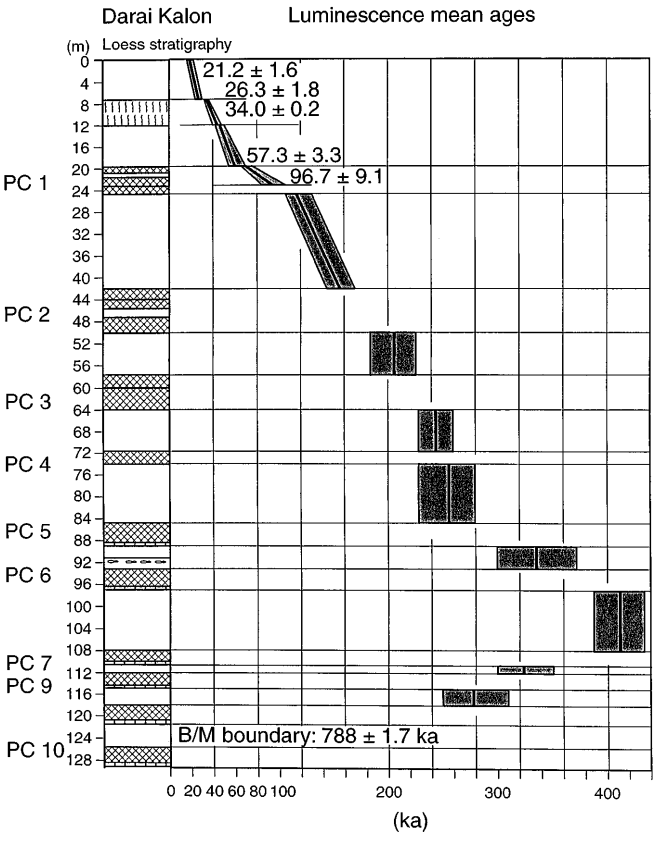

Fig. 12 Idealized sketch of TL/ADD dating results from the section at Darai Kalon. The Brunhes/Matuyama boundary is situated between PC10 and PC9 after Foerster and Heller (1994) and Pen`kov and Gamov (1980)

Sediments and loess of PC1

Two samples were taken from the middle part of the sediments of PC1 between the first (1) and second (2) dark-brown horizons (Fig. 4). The IRSL and TL dating results of the intercalated loess (sample DRK239) indicate a deposition age between 67 000±6100 and 73 900±6200 years. The lower one, sample DRK240, taken from the lower light brownish horizon indicates an age range from 66 300±6600 to 103 100±8500 years (Fig. 9). If compared with the oxygen-isotope record, the uppermost light brownish paleosol is equivalent to OI substages 5a or 5c. The intercalated loess represents a drier climatic event during OI substage 5a or represents OI substage 5b. It is most likely that the two dark-brown paleosols at the base of PC1 belong to OI substage 5e and, alternatively, the upper one to OI substage 5c. However, a correlation with the oxygen-isotope record is highly speculative because there are far too few data points from that part of the profile and thus do not allow a reliable correlation. More sampling and dating is required in order to get a better chronological resolution for the time interval of oxygen-isotope stage 5.

Loess between PC1 and PC5

The IRSL and TL age results show a similar behavior with depth (Figs. 5-9; Table 2). Age estimates determined by all applied methods are significantly underestimated for the loess between PC2 and PC5. The best age increase with depth was calculated using the TL additive dose method. The TL-ADD age estimates range from 117 000±9800 to 283 600±23 600 years for the samples taken from below PC1 down to PC5. However, a reliable and independent dating of single samples seems to be impossible due to scattering from sample to sample, which is most likely caused by a near saturation of the paleodose. A relative age increase is determinable, if the average age value for every loess cover is calculated (Fig. 12). However, the increase of the average age would require a very large data set and independent age information in order to apply a correction model.

Loess between PC5 and PC10

There is only a slight age increase for the samples investigated from below PC5. The data set does not improve the chronostratigraphic information about the section at Darai Kalon. The calculated age results are hypothetical and *only* of theoretical interest. The highest luminescence age estimates were determined for the loess from above PC6 down to the loess from below PC7 (samples DRK263-271). The older loess, although only three samples, shows

again anomalous behavior due to the near saturation level of the paleodose.

The upper age limit for the applied measuring conditions and the loess from the section at Darai Kalon is approximately 450000 years. An age underestimation of more than 60% for most of the oldest samples is likely, if compared with the independent age estimates of the B/M boundary between PC9 and PC10.

Conclusion

In Central Asia continuous dust/loess accumulation occurred between 65000 (70000 years) and approximately 20000 years in the Darai Kalon/Chashmanigar area. Different phases of higher and lower accumulation rates can be distinguished within the last interglacial/glacial cycle, indicating a close association with the global ice volume record. The maximum of dust/loess accumulation occurred between 20000 and 25000 years with average values of 1.20 m sediment thickness per 1000 years. Similar results were described from the upper pleniglacial of the last glaciation in Europe (Frechen 1991). Between 35000 and 28000 years the average dust accumulation rate was 0.78 m per 1000 years. The lowermost loess was deposited between 65000 and approximately 35000 years, resulting in a decreased average accumulation rate of 0.27 m per 1000 years. If a sediment accumulation rate is calculated for PC1 ("pedosedimentary model"), the result will be of the order of 0.10 m per 1000 years for the time span inclu-

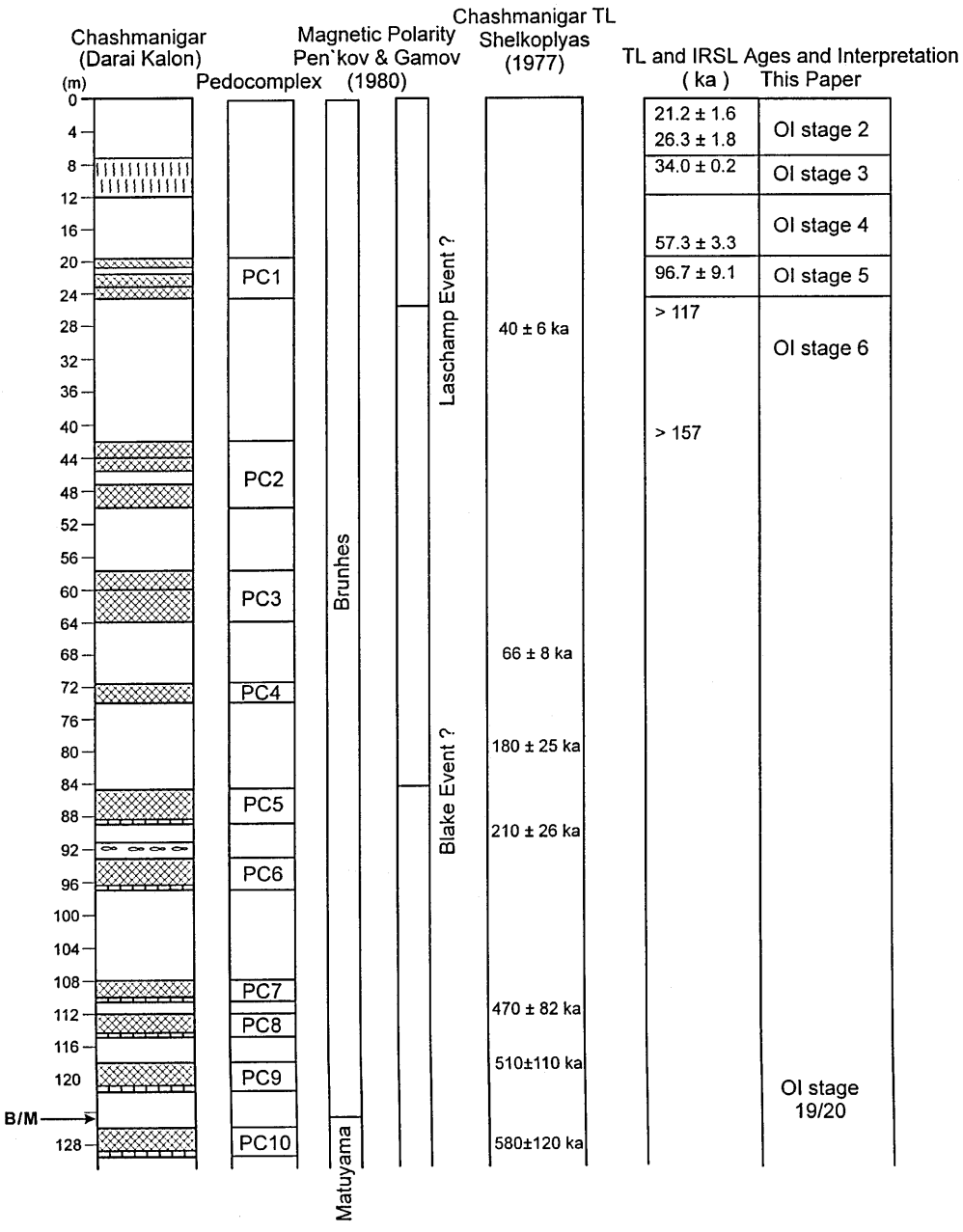

Fig. 13 Chronological interpretation of the Tadjic loess/paleosol sequences based on the data from the section at Darai Kalon. The data concerning the position of the Blake and Laschamp events and the early TL dating of the section at Chashmanigar are based on data from Dodonov et al. (1977) and Shelkoplyas (1977) that is no longer regarded as valid. The position of the Brunhes/Matuyama boundary was investigated by Foerster and Heller (1994) and Dodonov (unpublished data)

ding the complete oxygen-isotope stage 5. The determined accumulation rates are minimum values because the calculations do not take into account the loss by erosion processes. No distinct interstadial paleosol was found in the section at Darai Kalon, if compared with the European loess record. The uppermost part of the loess cover and the Holocene soil are truncated at Darai Kalon. The last interglacial pedocomplex is designated to be PC1 at the section at Darai Kalon; thus, PC1 has to be correlated with S1 of the Chinese loess stratigraphy (Fig. 13). The interpretation is of particular importance for the reconstruction of the human evolution in Central Asia resulting in much older age estimates for most of the archeological key sites in Tadjikistan, which are associated with PC5 and PC4 (Dodonov and Baiguzina 1995; Ranov 1995).

There is agreement between all applied methods for the IRSL and TL dating results above PC1. Sensitivity changes are negligible for the last glacial loess but increase systematically with depth for the older loess using both IRSL and TL dating methods. No age underestimation for IRSL and no extended scattering of the TL ages were found for the loess from Tadjikistan, whereas these problems were described from many loess sections in Europe (e.g., Frechen et al. 1995; Frechen, in press). A long-distance transport of the aeolian dust accumulated in the loess profile at Darai Kalon is most likely. This interpretation is supported by numerical agreement between IRSL and TL data sets of the last glacial loess and is supported by the grain-size distribution spectra of the sediments.

The upper numerical dating limit is determined to be 450000 years for the loess unit which includes the B/M boundary, for which an independent geological age of approximately 788000 years is available. However, a numerical upper dating limit does not mean that loess is absolutely datable as old as 450000 years. The data set of this study clearly indicates that under the applied experimental conditions, reliable IRSL and TL dating is only determinable for the last interglacial/glacial cycle – the past 130000 years! Systematic age underestimations of the order of 20–30% already occur for the penultimate glacial loess between PC2 and PC1. A significant improvement by application of a correction model, sensu Wintle (1990), does not improve the data set due to significant and increased sample-to-sample scattering of IRSL and TL age results with depth. A statistical trend analysis does improve the data set. However, up to now such a correction requires an extended data set and will be limited to loess sections for which at least one independent reliable dating record is available to calibrate and correct the luminescence age record.

Acknowledgements The dating study was carried out at the Luminescence Laboratory of the Geological Institute at the University of Cologne, Germany. The Fritz-Thyssen-Stiftung provided a grant to set up the luminescence dating laboratory. M. F. thanks the "Deutsche Forschungsgemeinschaft" for the financial support of the Tadjikistan project BO 413/10–1 (W. Boenigk) and for a habilitation grant (FR 877/4–1/2/3); W. Boenigk for discussions and his essential support of the project; R. Debuyst and F. Dejehet for their help and the permission to use the "INAN" irradiation facilities at the Université Catholique de Louvain, Belgium. We thank N. Shackleton and L. P. Zhou for fruitful discussions on the problems of geochronology of Central Asian loess, F. Chambers for comments on a previous version of the manuscript, and E. Oches and I. Smalley for constructive criticism and refereeing of the manuscript. We are very grateful to INTAS for supporting part of the field work.

References

Aitken MJ (1985) Thermoluminescence dating. Academic Press, London, pp 1–359

Aitken MJ (1992) Optical dating. Quaternary Sci Rev 11:127–131

Berg LS (1947) Climate and life. Isdanie 2. Geografgiz, Moscow, pp 1–356 (in Russian)

Boenigk W, Frechen M, Weidenfeller M (1994) Die mittel- und oberpleistozäne Deckschichtenfolge im Naturschutzgebiet "Eiszeitliches Lössprofil" in Koblenz-Metternich. Mainzer Geowiss Mitt 23:287–320

Bøtter-Jensen L, Ditlefsen C, Mejdahl V (1991) Combined OSL (infrared) and TL studies on feldspars. Nucl Tracks Radiat Meas 18:257–263

Bronger A, Winter R, Derevjanko O, Aldag S (1995) Loess-paleosol-sequences in Tadjikistan as a paleoclimatic record of the Quaternary in Central Asia. Quaternary Proc 4:69–81

Debenham NC (1985) Use of UV emissions in TL dating of sediments. Nucl Tracks Radiat Meas 10:717–724

Dodonov AE (1979) Stratigraphy of the Upper Pliocene–Quaternary deposits of Tadjikistan (Soviet Central Asia). Acta Geol Acad Sci Hung 22:63–73

Dodonov AE (1991) Loess of Central Asia. GeoJournal 24.2:185–194

Dodonov AE (1995) Geoarchaeology of Palaeolithic sites in loesses of Tadjikistan (Central Asia). In: Johnson E (ed) Ancient peoples and landscapes. Museum of Texas Tech Univ, Lubbock, Texas, pp 127–136

Dodonov AE, Baiguzina LL (1995) Loess stratigraphy of Central Asia: palaeoclimate and palaeoenvironmental aspects. Quaternary Sci Rev 14:707–720

Dodonov AE, Melamed YR, Nikiforova KV (1977) Guidebook for excursions. Int Symp on the Neogene–Quaternary Boundary, Nauka, Moscow, pp 1–184

Dodonov AE, Pen`kov AV (1977) Some data on the stratigraphy of the watershed loesses in Tadjic depression. Bull Comm Quaternary Res 47:67–76 (in Russian)

Dodonov AE, Ranov VA, Schäfer J (1995) Das Lösspaläolithikum am Obi-Mazar (Tadschikistan). Jahrb RGZ Mainz 39:209–243

Foerster T, Heller F (1994) Loess deposits from the Tajik depression (Central Asia): magnetic properties and paleoclimate. Earth Planet Sci Lett 128:501–512

Frechen M (1991) Thermolumineszenz-Datierungen an Lössen des Mittelrheingebiets. Universität zu Köln, Geologisches Institut, Sonderveröff 79:1–137

Frechen M (1992) Systematic thermoluminescence dating of two loess profiles from the Middle Rhine Area (F.R.G.). Quaternary Sci Rev 11:93–101

Frechen M (1995) The Upper Pleistocene terrestrial record: evidence from loess/paleosol sequences in Europe and Middle Asia. Terra Nostra 2:84

Frechen M (in press) The terrestrial record of the last interglacial/glacial cycle in Eurasia. Loess Lett (Suppl): 1–52

Frechen M, Preusser F (1996) Kombinierte Lumineszenz-Datierungen am Beispiel des Lössprofils Mainz-Weisenau. Frankfurter Geowiss Arbeit D20:53–66

Frechen M, Zhou LP (1995) Luminescence measurements of 780-ka-old loess samples from China. Abstracts of Luminescence and ESR Res Sem, University of Sussex, Brighton

Frechen M, Schweitzer U, Zander A (1996) Improvements in sample preparation for the fine grain technique. Ancient TL 14:15–17

Frechen M, Boenigk W, Weidenfeller M (1995) Chronostratigraphie des "Eiszeitlichen Lössprofils" in Koblenz-Metternich. Mainzer Geowiss Mitt 24:155–180

Frechen M, Horvath E, Gabris G (in press) Geochronology of Middle and Upper Pleistocene loess sections in Hungary. Quaternary Res 44: 291–312

Hütt G, Smirnov A (1984) Thermoluminescence dating in the Soviet Union. PACT 7:97–103

Kukla GJ, An Z (1989) Loess stratigraphy in Central China. Palaeogeogr Palaeoclimatol Palaeoecol 72:203–225

Lazarenko AA (1984) The loess of Central Asia. In: Velichko AA (ed) Late Quaternary environments of the Soviet Union. Longman, London, pp 125–131

Lazarenko AA, Bolikhovskaya NS, Semenov VV (1981) An attempt at detailed stratigraphic subdivision of the loess association of the Tashkent region. Int Geol Rev 23:1335–1346

Liu TS (1988) Loess and the environment. Springer, Berlin Heidelberg New York, pp 1–251

Liu TS (1991) Loess, environment and global change. Science Press, Beijing, pp 1–288

Mejdahl V (1988) Long term stability of the TL signal in alkali feldspars. Quaternary Sci Rev 7:357–360

Mejdahl V (1989) How far back: life times estimated from studies of feldspars of infinite ages. In: Aitken MJ (ed) Long and short range limits in luminescence dating. Research Lab for Archaeology and the History of Art, Oxford, Occas Publ 9, pp 53–58

Musson F, Wintle AG (1994) Luminescence dating of the loess profile at Dolni Vestonice, Czech Republic. Quaternary Geochron 13:411–416

Obruchev VA (1885) About the processes of weathering and deflation in Central Asia. Transact Mineral Soc 2/33, Issue 1:229–272 (in Russian)

Obruchev VA (1900/1901) Central Asia, northern China and Nan Shan. St. Petersburg, pp 1–2 (in Russian)

Obruchev VA (1911) To the questions on genesis of the loess (to defence of eolian hypothesis). Izvestia Tomskogo tekhnolog. Instituta, T.13, no. 1. Reprinted in Sel transact on Geography of Asia, T.3 Geografiz (1951), pp 197–242 (in Russian)

Obruchev VA (1948) Loess as a specific type of soil, its genesis and the tasks of study. Bull Comm Quaternary Res 12:5–17 (in Russian)

Pavlov AP (1903) On Turkestan and European loess. Byull. MOIP. N 4:43–67

Pécsi M, Richter G (1996) Löss: Herkunft – Gliederung – Landschaften. Z Geomorphol (NF Suppl) 98:1–391

Pen`kov AV, Gamov LN (1980) Paleomagnetic data on the Pliocene to Quaternary strata of southern Tadjikistan. The Neogene–Quaternary boundary. Nauka, Moscow, pp 189–194 (in Russian and English)

Pen`kov AV, Gamov LN, Dodonov AE (1976) Summary paleomagnetic section of the Upper Pliocene–Pleistocene deposits of the Kyzylsu river basin, South Tadjikistan. Izvestiya AN SSSR Ser Geol 9:33–43 (in Russian)

Pye K (1987) Aeolian dust and dust deposits. Academic Press, London, pp 1–334

Ranov V (1995) The “Loessic Palaeolithics” in South Tadjikistan, Central Asia: its industries, chronology and correlation. Quaternary Sci Rev 14:731–746

Richthofen FV (1878) Bemerkungen zur Lössbildung. Verh Geol Reichsanst, Berlin, pp 1–13

Schäfer J, Sosin PM, Ranov VA (1996) Neue Untersuchungen zum Lösspaläolithikum am Obi-Mazar, Tadzikistan. Archäol Korrespondenzbl 26:97–109

Shackleton NJ, An Z, Dodonov AE, Gavin J, Kukla GJ, Ranov V, Zhou LP (1995) Acumulation rate of loess in Tadjikistan and China: relationship with global ice volume cycles. Quaternary Proc 4:1–6

Shelkoplyas VN (1977) Thermoluminescence dating of subaerial Pleistocene deposits in Tadjikistan. In: Dodonov AE, Melamed YR, Nikiforova KV (eds) Guidebook for excursions. Int Symp Neogene–Quaternary Boundary. Nauka, Moscow, pp 120–122

Stepanov IN, Abdunazarov UK (1977) Buried soils in Middle Asian loess and their paleogeographical significance. Nedra, Moscow, pp 1–120 (in Russian)

Tauxe L, Herbert T, Shackleton NJ, Kok YS (1996) Astronomical calibration of the Matuyama-Brunhes boundary: consequences for magnetic remanence acquisition in marine carbonates and the Asian loess sequences. Earth Planet Sci Lett 140:133–146

Wintle AG (1985) Stability of the TL signal in fine grains from loess. Nucl Tracks Radiat Meas 10:725–730

Wintle AG (1990) A review of current research on TL dating of loess. Quaternary Sci Rev 9:385–397

Wintle AG (1994) Infrared-stimulated luminescence dating of sediments. Radiat Meas 23:607–612

Wintle AG, Huntley DJ (1982) Thermoluminescence dating of sediments. Quaternary Sci Rev 1:31–53

Zhou LP, Dodonov AE, Ranov V, Shackleton NJ (1995a) Loess in Central Asia: chronology and palaeoclimatic and archaeological significance. Terra Nostra 2:315

Zhou LP, Dodonov AE, Shackleton NJ (1995b) Thermoluminescence dating of the Orkutsay loess section in Tashkent region, Uzbekistan, Central Asia. Quaternary Proc 14:721–730